Highlights

- D-A-D type diphenylsulfone derivatives were synthesized.
- All compounds formed glasses with glass transition temperatures ranging from 68 to 162 ^{o}C.
- All hosts demonstrated high triplet energy levels of 2.99-3.08 eV.
- Hole-transporting properties with charge mobility exceeding 10^{-4} cm^2/Vs were estimated by time of flight technique.
- Bluish-green TADF OLEDs with EQE of 20% were fabricated.

Graphical abstract

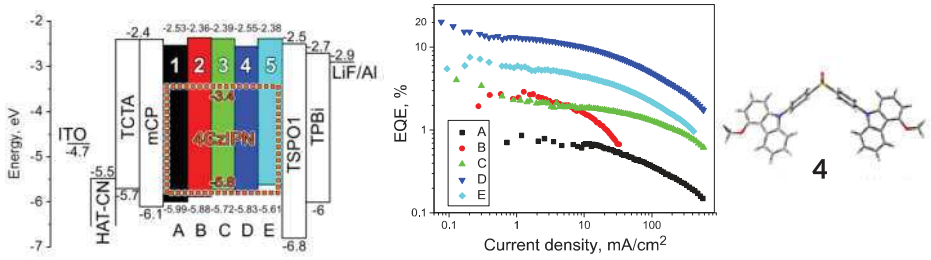

Diphenylsulfone-based hosts for electroluminescent devices: effect of donor substituents

Oleksandr Bezvikonnyi[a], Dalius Gudeika[a,b], Dmytro Volyniuk[a], Martins Rutkis[b], Juozas V. Grazulevicius[a*]

[a] *Department of Polymer Chemistry and Technology, Kaunas University of Technology, Radvilenu pl. 19, LT-50254, Kaunas, Lithuania*

[b] *Institute of Solid State Physics, University of Latvia, 8 Kengaraga St., Riga LV-1063, Latvia*

* *Corresponding author: juozas.grazulevicius@ktu.lt*

Abstract

In this work, we report on a series of diphenylsulfone derivatives substituted by 2-(trifluoromethyl)-phenothiazinyl, 10,11-dihydro-5*H*-dibenz[b,f]azepinyl, 5*H*-dibenz[b,f]azepinyl, 4-methoxy-carbazolyl and 1,2,3,4-tetrahydrocarbazolyl moieties. Utilization of such donating units provided high triplet levels (2.99-3.12 eV) of the designed compounds. The compounds were characterized by glass-forming properties (with glass transition temperatures of 68-162°C) and ionization potentials of 5.61-5.99 eV. Depending on the donor substitution pattern, either hole or electron transport was observed for the studied compounds with charge mobilities in the range from 5.3×10^{-6} to 2.8×10^{-4} cm^2/Vs at electric fields higher than $3.1\cdot10^5$ V/cm. Hosting properties of the compounds were studied using widely known emitter exhibiting thermally activated delayed fluorescence. Among the studied compounds, bis(4-(4-methoxy-9*H*-carbazole-9-yl)phenyl)sulfone showed the best performances in both guest:host solid films (photoluminescence quantum yield of 87%) and electroluminescent devices (maximum external quantum efficiency over 20%).

Keywords: diphenylsulfone, carbazole, TADF, host, OLED.

1. Introduction

The technology of organic light emitting diodes (OLEDs) [1] takes over the market of displays and lightning devices [2]. The spin-orbit coupling of phosphorescent dyes overcomes 25% limit of internal quantum efficiency by utilizing triplet excitons in emissive processes which usually are forbidden [3]. The high cost of rare-metal materials used as phosphorescent emitters is the greatest disadvantage of the approach of phosphorescent OLEDs. As the alternative, the concept of thermally activated delayed fluorescence (TADF) was proposed [4]. The main principle of the approach is tuning molecule characteristics in order to provide small singlet-triplet energy splitting facilitating reverse intersystem crossing of triplet excitons to the first singlet excited states with the following TADF [4].

Because of its electron-withdrawing property and geometry, diphenylsulfone is one of the most widely used acceptors in the design of deep blue TADF emitters [5]. The first series of such donor-acceptor-donor (D-A-D) compounds was introduced in 2012 [6]. However, diphenylsulfone-based host materials remain rare. Establishment of structural relationships with respect of effective energy transfer is crucial for a rational design of diphenylsulfone derivatives capable of operating as host materials for TADF OLEDs. In this context, seven-memberes cycles of donor moieties as well as other heterocyclic donors were used in the design of the potential hosts in order to study structure-properties relationship.

For testing of the ability of harvesting of TADF emission by host, it is more convenient to use green dopant than the blue one. (4s,6s)-2,4,5,6-Tetra(9*H*-carbazol-9-yl)isophthalonitrile (4CzIPN) as one of the most widely used green TADF emitter [7] was selected for this study. EQE of 19.3% was reported for OLED using this emitter [7]. 4CzIPN showed photoluminescence quantum yield (PLQY) above 90% and suitably short DF lifetime around 5μs and consequently enhanced TADF [7].

In this work, the newly synthesized donor-disubstituted diphenylsulfones were studied as potential hosts for 4CzIPN using not only experimental but also theoretical tools TADF OLED with an EQE over 20% based on one newly synthesized host is presented.

2. Experimental section

2.1 Materials

Bis(4-fluorophenyl)sulfone, 2-(trifluoromethyl)-10*H*-phenothiazine, 5*H*-dibenz[b,f]azepine, 10,11-dihydro-5*H*-dibenz[b,f]azepine and 1,2,3,4-tetrahydrocarbazole were purchased from Aldrich. 4-Methoxy-9*H*-carbazole (**I**, m.p. 137-138 ^{o}C) was synthesized according to the previously reported method [8].

2.2 Instrumentation

^{13}C NMR, ^{1}H NMR spectra were obtained using a Varrian Unity Inova (300 MHz (^{1}H) and 75 MHz (^{13}C)). Mass (MS) spectra, infrared (IR) spectra were recorded, elemental, thermogravimetric analysis (TGA), differential scanning calorimetry (DSC) measurements, absorption, photoluminescence (PL) spectra of dilute solutions and of the films, cyclic voltammetry (CV) measurements were recorded as described earlier [9]. Theoretical calculations had been carried with Gaussian 16 and Gaussview 6 softwares. Ionization potential measurements of the solid samples were performed by photoelectron emission method in air [10]. Electron and hole mobilities (μ_e, μ_h) were studied by time of flight technique [11]. OLEDs were fabricated by vacuum deposition of inorganic and organic layers onto cleaned ITO coated glass. Vacuum of 10^{-6} Torr was used. The active area of the obtained devices was 3×6 mm^2. The current density voltage and luminance voltage dependences were recorded with

semiconductor parameters analyzer (HP 4145A). Brightness was measured using a calibrated photodiode. Electroluminescence spectra were recorded with an Ocean Optics modular spectrometer.

2.3 Synthesis and characterization

Bis(4-(2-(trifluoromethyl)-phenothiazine-10-yl)phenyl)sulfone ***(1)***. 2-(Trifluoromethyl)-10*H*-phenothiazine (2.31 g, 8.65 mmol) was dissolved in *N*-methyl-2-pyrrolidone (15 mL). Bis(4-fluorophenyl)sulfone (1 g, 3.93 mmol), cesium carbonate (2.58 g, 7.93 mmol) were added into the mixture, and stirred under 170 °C using oil bath for 12 h. The mixture was cooled to room temperature and the product was extracted using methylene chloride. The organic layer was collected, filtered and evaporated to remove the solvent. The residue was purified by column chromatography using *n*-ethylacetate/*n*-hexane (8:1) as an eluent, crystallized from the mixture of ethylacetate and hexane to get **1** as light yellow crystals. FW = 748.78 g/mol, yield: 1.26 g, 43%; m.p. 283-284 ^{o}C. ^{1}H NMR (300 MHz, $CDCl_3$, δ, ppm): 7.88 (d, J = 8.1 Hz, 4H), 7.44 (d, J = 8.1 Hz, 2H), 7.39 – 7.30 (m, 4H), 7.24 – 7.20 (m, 4H), 7.19 – 7.12 (m, 6H), 7.01 (dd, J = 8.1, 1.0 Hz, 2H). ^{13}C NMR (75 MHz, $CDCl_3$, δ, ppm): 147.8, 141.9, 140.9, 136.1, 135.4, 129.7, 129.3, 128.7, 128.5, 127.7, 126.0, 124.0, 122.2, 120.3, 119.9. MS (APCI^{+}, 20 V), m/z: 750 ([M+H]$^{+}$). Elemental analysis calcd (%) for $C_{38}H_{22}F_6N_2O_2S_3$: C, 60.95; H, 2.96; F, 15.22; N, 3.74; O, 4.27; S, 12.85; Found: C, 60.99; H, 2.92; F, 15.18; N, 3.79.

Bis(4-(10,11-dihydro-5H-dibenz[b,f]azepine-5-yl)phenyl)sulfone ***(2)*** was synthesized according to the method similar to that used for the synthesis of **1**, except that 10,11-dihydro-5*H*-dibenz[b,f]azepine (1.68 g, 8.65 mmol) was used. The crude product was purified by column chromatography on silica gel using ethylacetate/*n*-hexane (7:1) as an eluent, crystallized from the mixture of ethylacetate and hexane to get the final derivative **2** as light yellow crystals. FW = 660.87 g/mol, yield: 1.06 g, 41%; m.p. 195-196 ^{o}C. ^{1}H NMR (300 MHz, $CDCl_3$, δ, ppm): 7.81 (dd, J = 8.7, 5.1 Hz, 4H), 7.52 (d, J = 9.0 Hz, 4H), 7.31 – 7.21 (m, 4H), 7.17 (d, J = 6.2 Hz, 4H), 7.04 (t, J = 8.6

Hz, 4H), 6.51 (d, J = 9.0 Hz, 4H), 2.88 (s, 8H). ^{13}C NMR (75 MHz, $CDCl_3$, δ, ppm): 165.7, 163.2, 152.6, 142.1, 139.2, 137.6, 131.2, 129.8, 129.5, 129.2, 129.0, 128.5, 128.0, 127.4, 116.3, 116.1, 112.3, 30.5. MS (APCI$^+$, 20 V), m/z: 662 ([M+H]$^+$). Elemental analysis calcd (%) for $C_{40}H_{32}N_2O_2S$: C, 79.97; H, 6.10; N, 4.24; O, 4.84; S, 4.85; Found: C, 79.93; H, 6.14; N, 4.19.

Bis(4-(5H-dibenz[b,f]azepine-5-yl)phenyl)sulfone ***(3)*** was synthesized according to the method similar to that used for the synthesis of **1**, except that 5*H*-dibenz[b,f]azepine (1.67 g, 8.65 mmol) was used. The crude product was purified by column chromatography on silica gel using ethylacetate/*n*-hexane (6:1) as eluent, crystallized from the mixture of ethylacetate and hexane to afford the final derivative **3** as light yellow crystals. FW = 656.83 g/mol, yield: 0.95 g, 37%; m.p. 377-378 ^{o}C. ^{1}H NMR (300 MHz, $CDCl_3$, δ, ppm): 7.43 – 7.26 (m, 20H), 6.74 (s, J = 8.5 Hz, 4H), 6.15 (d, J = 8.5 Hz, 4H). ^{13}C NMR (75 MHz, $CDCl_3$, δ, ppm): 151.9, 141.6, 135.7, 131.0, 130.5, 130.2, 129.9, 129.5, 128.3, 127.6, 111.4. MS (APCI$^+$, 20 V), m/z: 658 ([M+H]$^+$). Elemental analysis calcd (%) for $C_{40}H_{28}N_2O_2S$: C, 80.46; H, 5.52; N, 4.26; O, 4.87; S, 4.88; Found: C, 80.41; H, 5.56; N, 4.21.

Bis(4-(4-methoxy-9H-carbazole-9-yl)phenyl)sulfone ***(4)*** was synthesized according to the method similar to that used for the synthesis of **1**, except that 4-methoxy-9*H*-carbazole (1.70 g, 8.65 mmol) was used. The crude product was purified by column chromatography on silica gel using ethylacetate/*n*-hexane (8:1) as eluent and crystallized from the mixture of ethylacetate and hexane to afford the final derivative **4** as light yellow crystals. FW = 608.70 g/mol, yield: 1.55 g, 65%; m.p. 245-246 ^{o}C. ^{1}H NMR (300 MHz, $CDCl_3$, δ, ppm): 8.43 (d, J = 7.6 Hz, 2H), 8.28 (d, J = 8.7 Hz, 4H), 7.85 (d, J = 8.7 Hz, 4H), 7.48 (d, J = 8.2 Hz, 2H), 7.46 – 7.31 (m, 6H), 7.12 (d, J = 8.2 Hz, 2H), 6.81 (d, J = 8.2 Hz, 2H), 4.14 (s, 6H). ^{13}C NMR (75 MHz, $CDCl_3$, δ, ppm): 156.4, 142.8, 141.3, 139.3, 139.1 129.6, 127.2, 126.8, 125.4, 123.4, 122.5, 121.1, 113.2, 108.9, 102.4, 102.0, 55.6. MS (APCI$^+$, 20 V), m/z: 609 ([M+H]$^+$). Elemental analysis calcd (%) for $C_{38}H_{28}N_2O_4S$: C, 74.98; H, 4.64; N, 4.60; O, 10.51; S, 5.27; Found: C, 75.01; H, 4.59; N, 4.61.

Bis(4-(1,2,3,4-tetrahydrocarbazole-5-yl)phenyl)sulfone ***(5)*** was synthesized according to the method similar to that used for the synthesis of **1**, except that 1,2,3,4-tetrahydrocarbazole (1.48 g, 8.65 mmol)

was used. The crude product was purified by column chromatography on silica gel using ethylacetate/*n*-hexane (8:1) as eluent, crystallized from the mixture of ethylacetate and hexane to get **5** as light yellow crystals. FW = 556.72 g/mol, yield: 0.74 g, 34%; m.p. 219-220 ^{o}C. ^{1}H NMR (300 MHz, $CDCl_3$, δ, ppm): 8.06 (d, J = 8.6 Hz, 4H), 7.49 (d, J = 8.6 Hz, 4H), 7.45 – 7.40 (m, 2H), 7.26 – 7.19 (m, 2H), 7.14 – 7.00 (m, 4H), 2.64 (d, J = 5.4 Hz, 8H), 1.82 (d, J = 5.4 Hz, 8H). ^{13}C NMR (75 MHz, $CDCl_3$, δ, ppm): 142.8, 138.9, 136.5, 135.1, 129.1, 128.4, 127.1, 122.1, 120.6, 118.2, 113.1, 109.6, 23.6, 23.4, 22.8, 21.1. MS (APCI$^+$, 20 V), m/z: 557 ([M+H]$^+$). Elemental analysis calcd (%) for $C_{36}H_{32}N_2O_2S$: C, 77.67; H, 5.79; N, 5.03; O, 5.75; S, 5.76; Found: C, 77.71; H, 5.73; N, 4.98.

3. Results and discussion

3.1 Synthesis and characterization

Scheme 1 illustrates synthesis of **1-5**. The target compounds (**1-5**) were easily obtained in moderate yields by single step *via* nucleophilic cross-coupling reactions between bis(4-fluorophenyl)sulfone and the corresponding heterocyclic compound containing secondary amino group. ^{1}H NMR, ^{13}C NMR, elemental analysis, mass spectrometry were employed to validate the chemical structures of **1-5**. The derivatives were soluble in chloroform, dichloromethane, ethylacetate and other organic solvents.

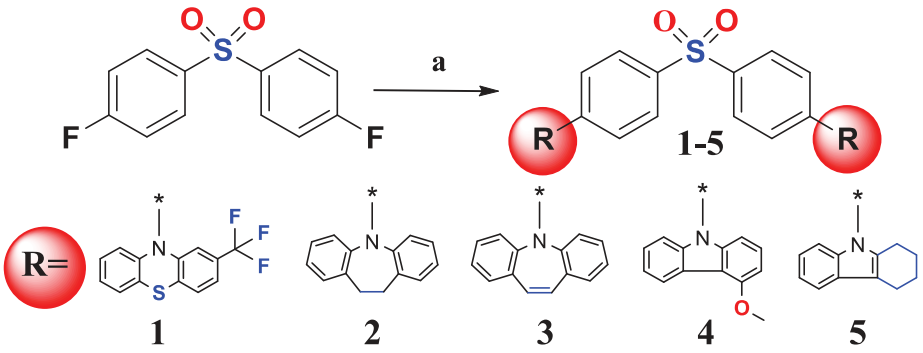

Scheme 1. Synthetic routed to **1-5.** Reagents and conditions: (a) 2-(trifluoromethyl)-10*H*-phenothiazine, 10,11-dihydro-5*H*-dibenz[b,f]azepine, 5*H*-dibenz[b,f]azepine, 4-methoxy-9*H*-carbazole or 1,2,3,4-tetrahydrocarbazole, Cs_2CO_3, NMP, 170 °C, 12 h.

3.2 Theoretical calculations

Density functional theory (DFT) calculations were executed to estimate geometries of the derivatives (**1-5**) at ground state (Figure 1). The dihedral angles between diphenylsulfone and 2-(trifluoromethyl)-phenothiazinyl moieties in compound **1** were found to be of ca. 71°. The large dihedral angles of **1** make the molecule highly twisted. In derivatives **4** and **5**, the dihedral angles between diphenylsulfone moiety and 1,2,3,4-tetrahydrocarbazolyl or 4-methoxy-carbazolyl moieties were 49 and 51°, respectively. The determined geometries of **1-3** resulted in the HOMO distribution on different donor substituents, whereas HOMO of compounds **4** and **5** were delocalized on the donor moieties extending to the diphenylsulfone units. LUMOs of **1, 4** and **5** were predominantly localized on the diphenylsulfone units, while in **2** and **3** LUMOs were shifted to the donor moieties.

The time-dependent DFT (TD-DFT) calculations allowed to predict excitation energies for derivatives **1-5** which are are given in Table S1 and Figure S6. The main transitions in compounds **1**, **4** and **5** are n-π* in nature, meanwhile transitions in compounds **2** and **3** are π-π* transitions. The strong absorption bands calculated at the B3LYP level were found at 418.83, 374.59 and 384.55 nm for **1**, **4** and **5**, respectively.

Due to the small dihedral angles between the acceptor and donor moieties, and a weak overlap of the HOMOs and LUMOs, **4** and **5** showed relatively high oscillator strengths of 0.2950 and 0.1343, respectively, indicating a highly facilitated radiative decay.

Compound	1	2	3	4	5
Optimized geometry	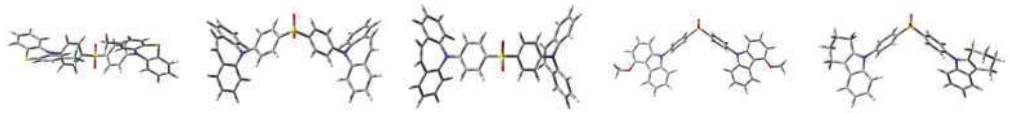				
HOMO					
LUMO					

Figure 1. Optimized geometries and HOMO/LUMO of derivatives **1-5** calculated at B3LYP/6-31(d,p) level in vacuum.

3.3 Thermal characterization

The thermal properties of derivatives **1-5** were estimated by thermogravimetric analysis (TGA) and differential scanning calorimetry (DSC) under nitrogen atmosphere. TGA curves are depicted in supporting information (Figure S7). The temperatures of 5% weight loss ($T_{d\text{-}5\%}$) of the derivatives were found to be enough high and ranged from 339 to 433 °C.

Table 1. Thermal characteristics of derivatives **1-5**.

Derivative	T_m, [°C][a] (scan rate of 10 °C/min)	T_g, [°C][b]	$T_{d\text{-}5\%}$, [°C][c] (scan rate of 20 °C/min)
1	288	103	385
2	199	68	339
3	382	162	433
4	251	141	406
5	224	121	405

[a] T_m - melting temperature (nitrogen atmosphere). [b] T_g - glass-transition temperature, second heating scan. [c] $T_{d\text{-}5\%}$ - 5% weight loss temperature (nitrogen atmosphere).

After the synthesis diphenylsulfone-based derivatives **1-5** were isolated as crystalline materials. As it was endorsed by DSC, they could be transmuted into molecular glasses by cooling their melts. DSC thermograms of derivative **3** are displayed in Figure 2. In the first heating scan the endothermal melting signal (T_m) of the sample of **3** was observed at 382°C. In the cooling scan any signal of crystallization was not observed. The second heating scan demonstrated glass transition (T_g) at 162 °C. The analogous behaviour in DSC experiments was observed for derivatives **1**, **2**, **4** and **5**. When the samples of **1**, **2**, **4** and **5** were heated they showed endothermic T_m signals at 288, 199, 251 and 224 °C, respectively. In the second heating scans the derivatives showed relatively T_g at 103, 68, 141 and 121 °C, respectively. Glass transition temperatures of derivatives **1** and **3-5** having 2-(trifluoromethyl)-phenothiazinyl, 5*H*-dibenz[b,f]azepinyl, 4-methoxy-carbazolyl and 1,2,3,4-tetrahydrocarbazolyl moieties was found to be higher by 35, 94, 73 and 53 °C than that of derivative **2** containing 10,11-dihydro-5*H*-dibenz[b,f]azepinyl substituent. This observation can be explained by the weaker intermolecular interaction in the sample of **2.**

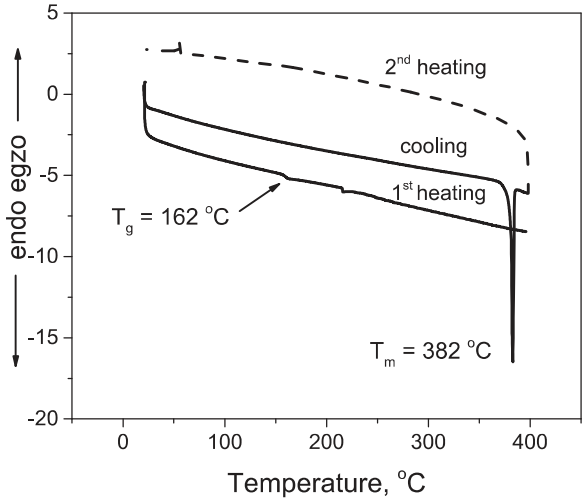

Figure 2. DSC thermograms of compound **3**.

3.4 Photyphysical properties

UV absorption, photoluminescence (PL) spectra of neat films and dilute solutions of the studied derivatives recorded at room and liquid nitrogen temperature are presented in Figure 3. Position of the main absorption spectral peak at low-energy wavelength depends strongly to the type of donor substituents. At the same time, the influence of diphenylsulfone moiety on absorption spectra of compounds **1-5** was practically not detectible. The low-energy absorption peaks of the films appeared at 302 nm for **3**, at 306 nm for **2,** at 317 nm for **1,** at 337 nm for **4** at 340 nm for **5** strongly depending on the conjugation of the donors. Exploration of the possibility of solvatochromism was additionally performed (Figures S8-12). The absence of significant correlation with the solvent polarity showed no substantive charge transfer (CT) nature of absorption. The obtained experimental data are in accordance with the theoretical absorption spectra obtained by means of TD-DFT calculation (Figure S6). The absorption spectra of neat films and toluene solutions of the derivatives were practically identical. As expected, the absorption spectra of **4** and **5** consisted of sharp peaks with the highest oscilator strength (Table S1) for the $S_0 \rightarrow S_1$ excitation at ~340 nm attributed to the HOMO-LUMO transition. In contrast, the main broad absorption bands of **1, 2** and **3** correspond to the high energy $S_0 \rightarrow S_{3,4}$ transitions. Absorption spectra of the samples of **2** conform to the absorption of the 10,11-dihydro-5*H*-dibenz[b,f]azepinyl moiety [12], however, with a bathochromic shift to 305 nm. Partial LUMO localization on donor moieties in the case of **2** and **3** points to contribution of local excited (LE) states to various π-π* transitions and the red-shift of the UV spectrum of **2**. E_g^{opt} values of 2.53, 2.36 2.39, 2.55 and 2.38 eV for **1-5**, respectively, were taken from the absorption spectra onsets of the films and were used as the closest representation of a HOMO-LUMO gap for approximate estimation of the energy levels of frontier molecular orbitals of compounds by substraction of E_g^{opt} from IP values (Table 3).

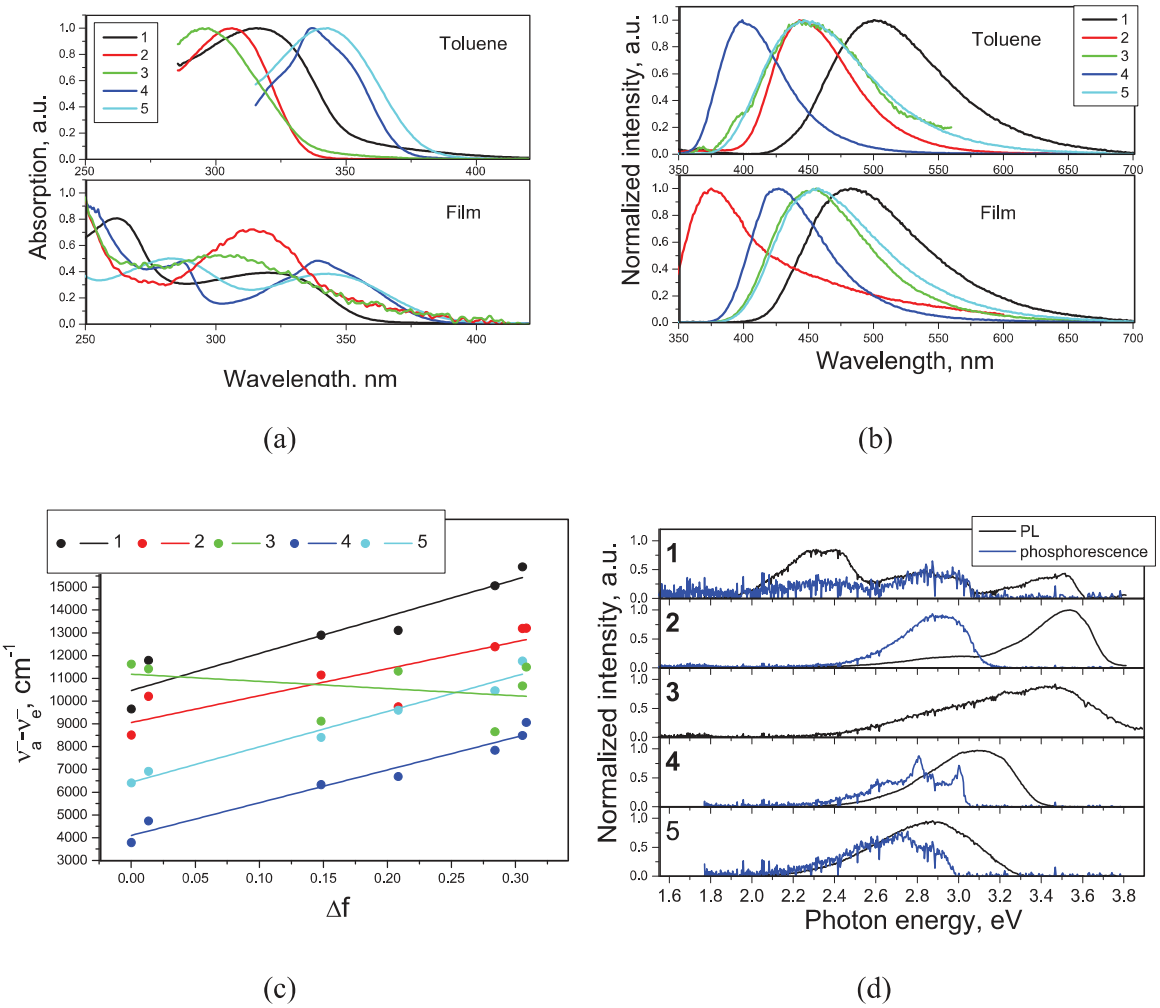

Figure 3. 1-5: (a) Absorption spectra of neat thin films and dilute toluene solutions. (b) PL spectra of neat thin films and dilute toluene solutions. (c) Lippert-Mataga plot showing the relation between Stokes shift and orientation polarisability of the different solvents. (d) PL and phosphorescence spectra of dilute THF solutions recorded at 77 K.

The Onsager description of non-specific electrostatic interactions between solvent and solute gives a pass to theories of solvatochromic effect in absorption and emission spectra [13]. The Lippert-Mataga plots [14] for **1-5** based on relation of the Stokes shift $\Delta\tilde{\nu}$ and orientation polarizability Δf defined as $\Delta\tilde{\nu} = \frac{2\Delta f}{4\pi\varepsilon_0\hbar c a^3}(\mu_e - \mu_g)^2 + \Delta\tilde{\nu}^0$ are presented in Figure 5c. Superscript ^{0} is an indication of the absence of solvent. a stands for the Onsager cavity radius. The slope for **3** was found to be negative and close

to 0. This is due a fact that no strong correlations between solvent polarity and peak positions appeared for the derivaitve. The assumptions of the Lippert-Mataga approach requires a linearity and a positive value of the slope [15]. It cannot be applied for a description of **3**. We can assume that this compound has a zero dipole moment. For the purpose of better fit, the data for polar protic methanol solution of **5** was excluded from the plotting. The CT-character of emission of **1**, **2**, **4** and **5** in a polar medium is evidenced by the monotonical bathochromic shift of PL spectral peak with increasing solvent polarity (hexane (Δf = 0.0001) → toluene (Δf = 0.0135) → chloroform (Δf = 0.1483) → tetrahydrofuran (Δf = 0.2085) → acetone (Δf = 0.284) → acetonitrile (Δf = 0.3055) → methanol (Δf = 0.3086). The approximated slopes for these compounds (Table 2) with linear relationships (R-square coefficients are from 0.69 to 0.96) corresponds to the $(\mu_e - \mu_g)^2$, reveal the changes of dipole moments after excitation. The obtained values correlate well with the theoretical predictions and disclose the intramolecular CT nature of emission. High electronegativity of CF_3 and metoxy- groups indicates a strong electron withdrawing as the major cause of this observation for **1** and **4**. The geometry of **2** leads to slightly smaller differences of the dipole moments in the excited μ_e and ground μ_g states.

Table 2. Photophysical data derived from spectral measurements.

Compound	Φ_{THF}[a]	Φ_{tol}[a]	Φ_{film}[b]	Φ_{4CzIPN}[c]	Lifetimes[d], ns	Slopes[e], 10^3 cm^{-1}	E_g^{opt}[f], eV	E_{S1}[g], eV	E_{T1}[g], eV	ΔE_{ST}[g], eV
1	0.02	0.02	0.12	0.22	1.8, 4.2	16.2	2.53	3.60 (2.96)	3.08 (2.85)	0.52 (0.11)
2	0.56	0.33	0.2	0.76	0.5, 6.4	11.8	2.36	3.73 (3.17)	3.12 (2.66)	0.61 (0.51)
3	~0.0001	~0.0001	0.13	0.29	3.5, 13.7, 36.9	-3.2	2.39	3.87 (3.14)	- (2.66)	- (0.48)
4	0.49	0.43	0.49	0.87	4.9, 11.3	14.4	2.55	3.38 (3.31)	3.03 (3.01)	0.35 (0.30)

5	0.22	0.33	0.27	0.28	3.5, 11.5	15.5	2.38	3.29 (3.22)	2.99 (2.95)	0.30 (0.27)

[a)] PLQY values of deoxygenated dilute solutions of compounds. [b)] PLQY values of neat films of compounds. [c)] PLQY values of thin films of 4CzIPN doped in compounds (5wt%). [d)] Calculated from PL decay curves of neat films of compounds (Figure S13). [e)] Slopes of Lippert-Mataga plots. [f)] E_g^{opt} is the onset wavelength of UV absorption spectrum of films. [g)] Estimated from onsets of emission spectra of dilute tetrahydrofuran solutions recorded at 77 K. The theoretical values of E_{T1}, ΔE_{ST}, E_{S1} are depicted in parentheses.

PL spectra of the films correlate to a great extent with PL spectra of dilute toluene solutions with insignificant spectral shifts. The only exclusion is the film of **2** which exhibited major PL peak assigned to LE emission with a CT-tail. The other films emit in a blue spectral range. As one of the direct results of extremely high torsion angles between the diphenylsulfone and 2-(trifluoromethyl)-phenothiazinyl moieties and consequent decreased values of oscillator strength of $S_0 \rightarrow S_{1\text{-}2}$ excitation transitions, PLQY of the film and of deoxygenated solutions of **1** are the lowest in the series of the films and solutions of the studied compounds (Table 2). The evidence of the phenomenon of aggregation induced emission (AIE) [16] is postulated from the PLQY increase of **3** from practically zero for dilute deoxygenated solutions to 13% for a solid sample. The restriction of intramolecular vibrational and rotational motion is the reason of the AIE [17,18]. PL lifetime values derived from fitting a reconvolution of exponential functions of the PL decay curves of neat films can be attributed to prompt fluorescence. Energy levels of the first singlet and triplet excited states of studied compounds were calculated from onsets of PL and phosphorescence spectra, respectively, of their frozen dilute THF solutions (Figure 3d). Due to extremely weak phosphorescence, spectrum and corresponding E_{T1} value for **3** were not obtained. The singlet and triplet excited state geometries were calculated using TD-DFT. The triplet levels (E_{T1}) of derivatives estimated both experimentally and theoretically were found to be reliant on E_{T1} of the donors. The values of E_{T1} of **1, 4** and **5** having 2-

(trifluoromethyl)-phenothiazinyl, 4-methoxy-carbazolyl and 1,2,3,4-tetrahydrocarbazolyl moieties were found to be higher than 2.85 eV. The energy spitting ΔE_{ST} between first singlet and triplet excited states were found to be in order of 0.30-0.61 eV.

3.5 Photyphysical properties of host-guest systems

Bipolar compounds **1-5** having triplet energy levels higher than 3 eV can be good candidates for being host materials. In order to provide comparable study of hosting properties of the developed derivatives **1-5** for TADF dopants, thin host-guest films with 5wt% concentration of 4CzIPN were prepared. TADF emitter 4CzIPN was selected since its triplet energy level of 2.4 eV [19] are considerably lower than those of **1-5** for efficient harvesting of triplet excitons and its HOMO and LUMO values match well those of **1-5** [7]. Absorption and PL spectra of the doped films are presented in Figure 4a. Absorption spectra of the samples conform to the respective absorption spectra of films of the derivatives. However, the low energy bands (LEB) of absorption at ~375 nm with a low intensity caused by small transition dipole moments the films of molecular mixtures 4CzIPN:**1**, 4CzIPN:**2**, 4CzIPN:**3** are related to $S_0 \rightarrow S_{1,2}$ transitions of hosts predicted by theoretical investigation (Table S1, Figure S6). They were well spectrally resolved (Figure 3a) due to impact of guest/host interactions on the positions of molecular orbitals. The broad tails in the range from ca. 420 nm to ca. 590 nm are ascribed to CT processes. While absorption spectra of the doped films correspond to those the compounds **1-5**, PL spectra correspond to 4CzIPN emission. This observation affirms the electronic excitation energy transfer from the host to the guests. This is due the fact that PL spectra of most of the studied compounds matched with absorption of 4CzIPN [20].

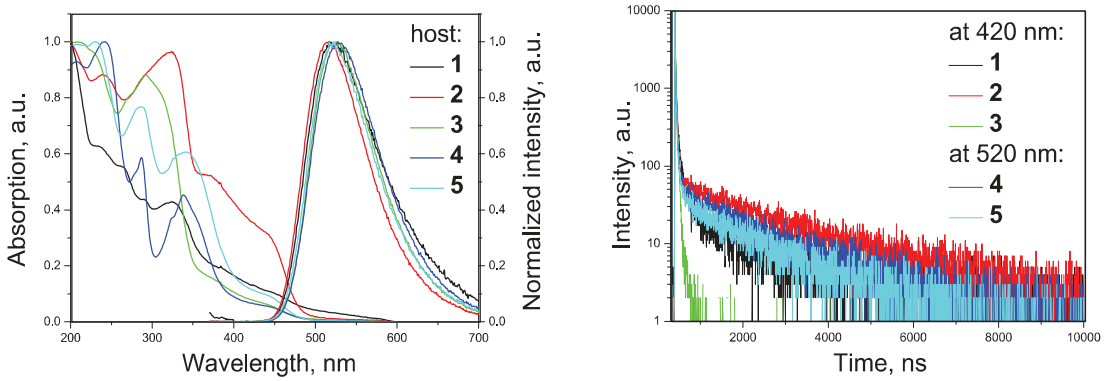

(a) (b)

Figure 4. Absorption and PL spectra (a) and PL decay curves of thin films of 5wt% solid solutions of 4CzIPN in **1-5**.

PL peak positions of the host-guest systems are slightly affected by the polarity of the host materials being in the order of **1>5>4>2>3** as it is for slopes of Lippert-Mataga plots (Figure 3c, Table 2). PL decay curves of the molecular mixtures of the same weight concentration are shown in Figure 4b. Low polarity of the host leads to the smallest DF lifetime for the system 4CzIPN:**3** in the series as the result of absence of CT. Correspondingly, PLQY of this guest:host system is as low as 29%. Due to unfavorable HOMO distribution of **5**, the PLQY value of the system 4CzIPN:**3** is almost the same. HOMO localization on donor units of compounds **2** and **4** facilitates CT leading to the longest emission lifetimes (in μs range) and the highest PLQY values of 76 and 87% of the films of 4CzIPN doped in **2** and **4**, respectively. The PLQY value of the film of 87% for 4CzIPN(5 wt%):**4** is even slightly higher than that 83% observed for the film of 4CzIPN(5 wt%):4,4'-bis(carbazol-9-yl)biphenyl (CBP) [7].

3.6 Electrochemical and photoelectrical properties

The electrochemical characteristics of compounds **1-5** were studied by cyclic voltammetry (CV). Derivatives **1-5** showed single oxidation peaks, which can be intended to oxidation of

electron rich 2-(trifluoromethyl)-phenothiazinyl, 10,11-dihydro-5*H*-dibenz[b,f]azepinyl, 5*H*-dibenz[b,f]azepinyl, 1,2,3,4-tetrahydrocarbazolyl or 4-methoxy-carbazolyl moieties, respectively. Derivatives **1, 4** and **5** exhibited slightly lower oxidation potential than **2** and **3**. This result indicates that 2-(trifluoromethyl)-phenothiazinyl, 1,2,3,4-tetrahydrocarbazolyl or 4-methoxy-carbazolyl moieties exhibit stronger electron-donating character as compared to that of 10,11-dihydro-5*H*-dibenz[b,f]azepinyl, 5*H*-dibenz[b,f]azepinyl moieties (Figures 5, S14).

Table 3. Oxidation potential, HOMO/LUMO energies, electron affinities, ionization potentials and of derivatives **1-5**.

Derivative	E_{onset}^{ox} vs Fc, [V]	IP_{CV}[a], HOMO[c] [eV]	EA_{CV}[b], LUMO[c] [eV]	E_g^{opt}, [eV][d]	I_p^{PES}, [eV][e]	I_p^{PES}, [eV][f]
1	0.54	5.35/-5.41	1.85/-1.87	3.50	5.99	2.53
2	0.82	5.74/-5.29	2.02/-1.48	3.72	5.88	2.28
3	0.78	5.69/-5.29	2.06/-1.47	3.63	5.72	2.15
4	0.58	5.41/-5.41	2.06/-1.60	3.35	5.83	2.56
5	0.31	5.03/-5.35	1.78/-1.63	3.25	5.61	2.41

[a] $IP_{CV} = |-(1.4\times 1e^{-}\times E_{onset}^{ox}$ *vs* Fc/V) − 4.6| eV [21]. [b] $EA_{CV} = -(|IP_{CV}|-E_g^{opt})$ (E_{onset}^{ox}- onset oxidation potential *vs.* the Fc/Fc^{+}. [c] Theoretically estimated HOMO/LUMO levels. [d] $E_g^{opt} = 1240/\lambda_{edge}$, where λ_{edge} is the onset wavelength of UV absorption spectrum of the dilute toluene solution (Table 2). [e] I_p^{PES} is the ionization potential of thin solid layers estimated by photoelectron emission spectrometry. [f] E_A^{PES} is electron affinity for the samples in solid-state.

According to the procedure reported earlier [21], ionization energy (IP_{CV}) values were estimated using the equation $IP_{CV} = |-(1.4\times 1e\times E_{onset}^{ox}$ vs Fc/V) − 4.6| eV. The values of IP_{CV} are listed in Table 3. They ranged from 5.03 to 5.74 eV. Derivative **5** having 1,2,3,4-

tetrahydrocarbazole moiety showed the lowest value of IP_{CV}. Electron affinities (EA_{CV}) estimated from the optical band gaps (E_g^{opt}) and IP_{CV} values were found to range from 1.78 to 2.06 eV.

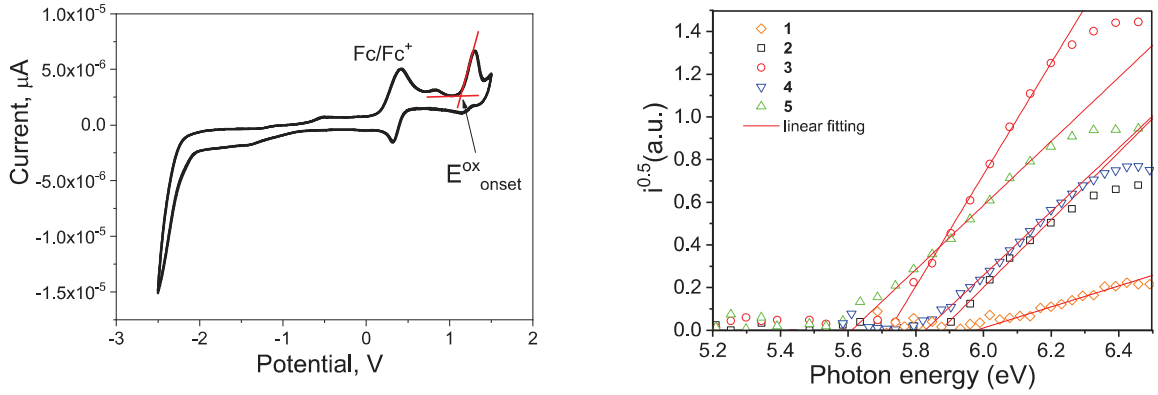

(a) (b)

Figure 5. (a) Cyclic voltammograms of dilute solution of derivative **3** in dry dichloromethane (scan rate 100 mV/s). (b) Electron photoemission spectra of compounds **1-5** recorded in air.

Electron photoemission spectrometry (PES) was exploited for getting ionization potentials (I_p^{PES}) of compounds **1-5** in solid-state. The values of I_p^{PES} are collected in Table 3. They were taken at crossing points of abscissa axis with extrapolated linear parts of low-energy edges of the corresponding photoelectron emission spectra (Figure 5b). Using optical band-gap energies (E_g) taken from absorption spectra of vacuum-deposited films, electron affinities (E_A^{PES}) of the solid samples of **1-5** were calculated by the formula $E_A^{PES} = I_P^{PES} - E_g$ (Table 3). Because of the different donating abilities of the donor moieties, the values of I_p^{PES} and E_A^{PES} for the studied diphenylsulfone derivatives were found in the ranges of 5.61-5.99 and 2.15-2.56 eV, respectively. I_p^{PES} and E_A^{PES} values of the compounds are suitable for their usage as OLED hosts. Both efficient charge-injection from electrodes and efficient exciton transfer from the host to the guest may be expected exploiting appropriate device structures and OLED emitters [22].

3.7 Charge-transporting properties

To estimate the potential of compounds **1-5** as OLED hosts, their charge-transporting properties were investigated by time-of-flight (TOF) method. Applying electric fields of different polarity, photocurrent transients for holes or electrons for vacuum-deposited films of compounds **1-5** were recorded (Figure S15). Transit times for both holes and electrons at different electric fields could be clearly determined from the plotted in log-log scales corresponding photocurrent transients of the layer of compound **5** show in Figures 6a,b. This finding indicates bipolar charge-transporting properties of derivative **5.** The same properties were detected for compound **3**. In case of compound **4,** only hole-transporting properties were proved by TOF technique since transit times for electrons were not well visible (Figure S15). Neither hole nor electron transport was proved for the layers of compounds **1** and **2**. The corresponding transit times were not well detectable from the photocurrent transients (Figure S15). Difficulties to determine transit times for holes/electrons in the films of compounds **1** and **2** may be explained either by the strong charge-transport dispersity which is evident from the shapes of their photocurrent transients or by higher relaxation times of photogenerated charges than the TOF transit times.

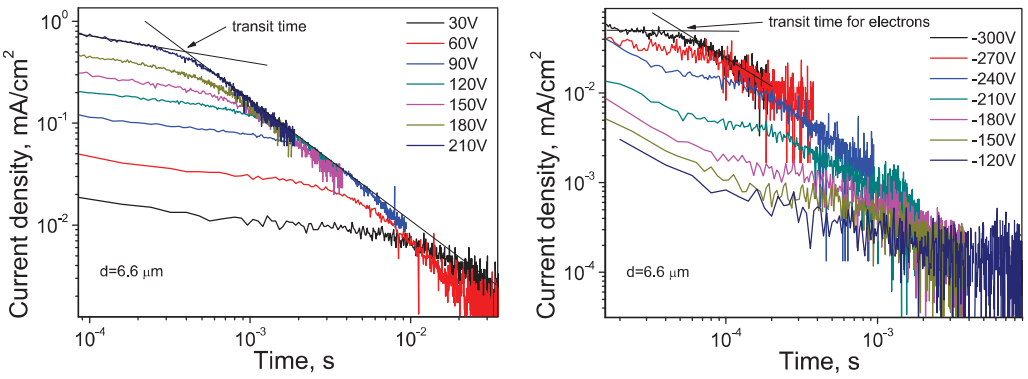

(a) (b)

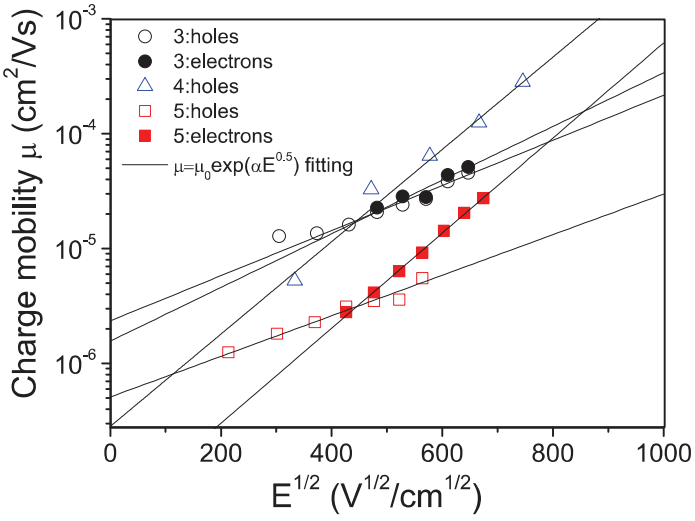

(c)

Figure 6. Photocurrent transients of holes (a) and electrons (b) for vacuum-deposited film of compound **5** and electric field dependences of charge mobilities for the layers of compounds **3-5** (c). Fitting was performed according Poole–Frenkel type mobility ($\mu = \mu_0 e^{\alpha E^{0.5}}$ where μ_0 is zero-field mobility; α is field dependence parameter, and E is electric field [23].

4-Methoxy-9*H*-carbazole-substituted diphenylsulfone derivative **4** showed the highest hole mobility reaching 2.8×10^{-4} cm^2/Vs at electric field of 5.6×10^5 V/cm (Figure 6c). Lower value of hole mobility of 4.6×10^{-5} cm^2/Vs at the same electric field was observed for derivative **3**. At the same electric field, only slightly higher value of electron mobility of 5.1×10^{-5} cm^2/Vs was observed for compound **3** indicating charge transport balance required for OLED hosts [9,24]. Derivative **5** showed hole and electron mobilities of 5.3×10^{-6} and 9.1×10^{-6} cm^2/Vs respectively at electric field of 3.1×10^5 V/cm. Decrease of charge mobilities in the range **4**>**3**>**5** reflects the effect of different donor substituents on charge-transporting properties of *para*-substituted diphenylsulfone derivatives. Charge mobilities of compounds **1** and **2** may be even lower than those of **3-5**. Thus, 4-methoxy-9*H*-carbazole-based compound **4** demonstrated the highest hole mobility among the studied compounds

3.8 Device fabrication and characterization

Series A-E of OLEDs with the structure of ITO/HAT-CN (4 nm)/TCTA (40 nm)/mCP (10 nm)/4CzIPN:host (5wt%, 30 nm)/TSPO1 (4 nm)/TPBi (45 nm)/LiF (0.6 nm)/Al with **1-5** as hosts, respectively, were fabricated and analyzed with the purpose of testing TADF host capabilities of the compounds. The energetic diagram representating energy levels of frontier orbitals of the respective organic materials is presented in Figure 7a. Major electroluminescent data of OLEDs A-E are showed in Table 4 and shown in Figure 7, S16-S20. The layers of 1,4,5,8,9,11-hexaazatriphenylenehexacarbonitrile (HAT-CN) and LiF were used for the injection of charge carriers. The layers of 4,4',4"-tris(carbazol-9-yl)triphenylamine (TCTA) and 2,2',2"-(1,3,5-benzinetriyl)-tris(1-phenyl-1-*H*-benzimidazole (TPBi) were employed as hole and electron transporting layers, respectively. 1,3-Di(9*H*-carbazol-9-yl)benzene (*m*CP) was taken for the fabrication of exciton blocking layer. Second exciton blocking layer of diphenyl[4-(triphenylsilyl)phenyl]phosphine oxide (TSPO1) was also used for the blocking of hole penetration into the layer of TPBi. Electrodes were the layers of indium-tin oxide (ITO) and aluminium (Al).

As it could be predicted from the highest PLQY value at 87% of the respective doped films containing compound **4** of the same weight concentration, device D based on compound **4** exhibited the best results from the series with maximum EQE over 20%, luminance of 28.9 thousand cd/m^2 and CIE color index best representing 4CzIPN emission (Figure 7 b-d, Table 4) [25]. This result was partly contributed by the highest charge mobility of compound **4** (Figure 6c). Efficiency of device B with the host material **2** was found to be much lower, apparently, due to lower charge carriers mobilities of **2**.

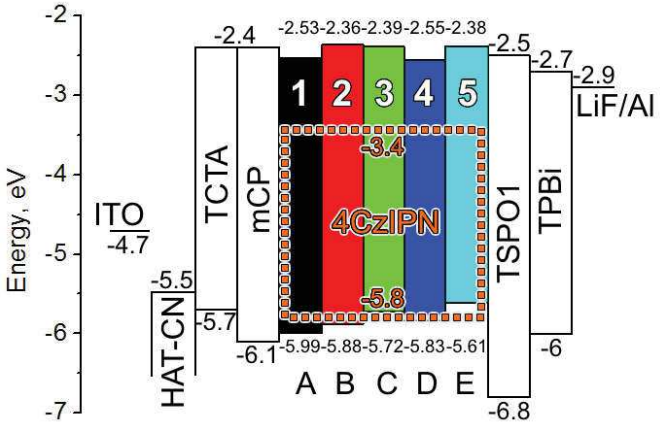
Energy, eV
-2
-3
-4
-5
-6
-7
ITO
-4.7
HAT-CN
-5.5
TCTA
-2.4
-5.7
mCP
-6.1
-2.53-2.36-2.39-2.55-2.38
1
2
3
4
5
-3.4
4CzIPN
-5.8
-5.99-5.88-5.72-5.83-5.61
A B C D E
TSPO1
-2.5
-6.8
TPBi
-2.7
-6
LiF/Al
-2.9

(a)

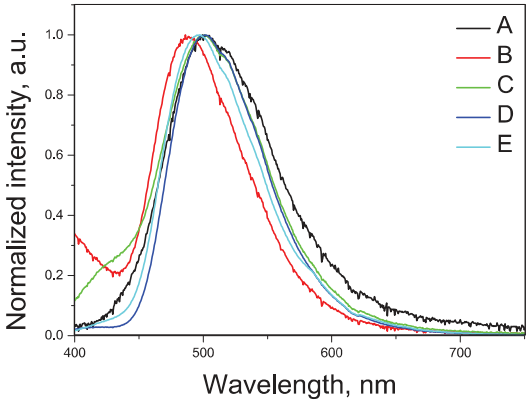
Normalized intensity, a.u.
1.0
0.8
0.6
0.4
0.2
0.0
400
500
600
700
Wavelength, nm
A
B
C
D
E

(b)

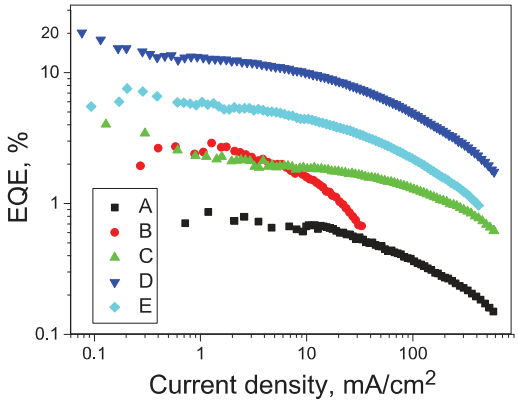
EQE, %
20
10
1
0.1
0.1
1
10
100
Current density, mA/cm2
A
B
C
D
E

(c)

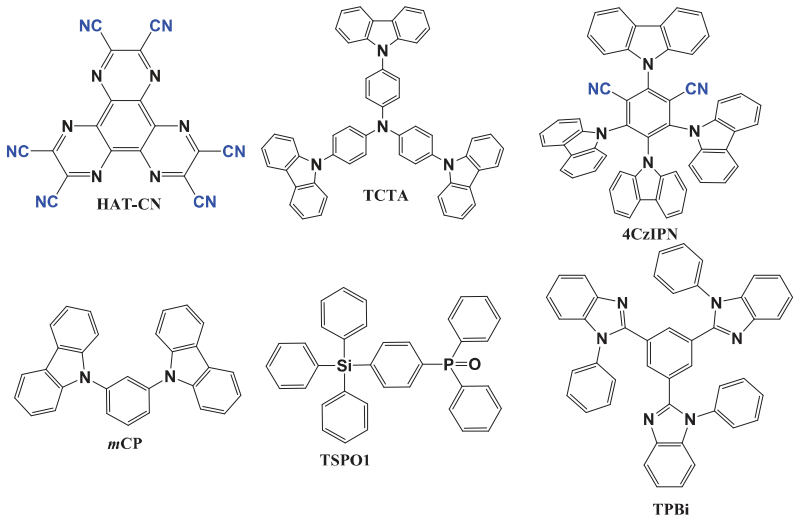
NC
CN
HAT-CN
TCTA
4CzIPN
mCP
TSPO1
Si
P=O
TPBi

(d)

Figure 7. Energy level diagram of the materials of organic layers of OLEDs A-E estimated from the E_g^{opt} and IP values (a), EL spectra recorded at 9 V (b) EQE-current density characteristics (c) and molecular structures of the organic compounds used in the devices (d).

Bluish-green electroluminescence with similar 1931 CIE chromaticity coordinates was recorded for the fabricated devices A-E (Figure 7b, Table 4). EL spectra of the devices are mainly attributed to emission of the used guest 4CzIPN [8]. Because of the differences in dipole moments of the designed hosts **1-5** which are evident from the slopes of Lippert-Mataga plots decreasing in the row **1>5>4>2>3** (Figure 3c, Table 2), all the fabricated devices showed the host contribution into emission slightly influencing 4CzIPN-related spectral peak position. High-energy band peaked at 385 nm attributed to emission of host **2** was observed in EL spectra of device B (Figure S17). This observation indicates weak host-guest energy transfer in the light-emitting layer of device B. Similarly, the high-energy shoulder (because the host emission) was observed in EL spectra of device C due to the weak host-guest energy transfer (Figure 7b). As a result, lower maximum EQEs of 2.9 and 4% were obtained for devices B and C in comparison to that of device D with efficient host-guest energy transfer in its light-emitting layer (Figure 7c, Table 4). The TADF quenching observed from a PL decay curve (Figure 4b) was apparently the reason of relatively low EQE of 4% observed for device C. Emission of hosts were practically not observed in EL spectra of devices A and E. However, their corresponding maximum EQE values (0.8 and 7.6%) were also lower than that of device D. This results can be mainly explained by 1) the lower PLQYs (22 and 28%) of the light-emitting layers of 4CzIPN:**1** and 4CzIPN:**5** than that (87%) of 4CzIPN:**4** due to the higher polarity of the hosts **1** and **5** in comparison to the polarity of **4** (Table 2); and 2) the lower charge mobility at least of host **5** in comparison to that of host **4** (the charge mobility of host **1** was most probably also lower than that of host **4** but this was not proved by TOF measurements) (Figure 6c). Meanwhile, the “perfect” relationship between charge-transporting/-injecting properties, appropriate [26] polarity and rigidity resulted in the high PLQY value of the guest 4CzIPN and efficient host-guest energy transfer occurred in the case of host

4. Therefore, the highest maximum EQE of 20.1% was obtained for device D in comparison to those of all other fabricated devices despite the same device structure and the same TADF emitter used. These findings well demonstrate effect of different donor substituents of diphenylsulfone-based hosts on out-put characteristics of electroluminescent devices highlighting potential of diphenylsulfone- and 4-methoxy-9*H*-carbazole-based host **4**.

Table 4. Characteristics of OLEDs.

Device	Host	L_{max}[a], 10^3 cd/m^2	EQE_{max}[b], %	PE_{max}[c], lm/W	CE_{max}[d], cd/A	$CIE_{x,y}$[e]
A	**1**	2.2	0.8 (0.7)	0.9 (0.7)	2.1 (1.7)	(0.23, 0.43)
B	**2**	0.5	2.9 (2.7)	2.9 (2.6)	6.0 (5.7)	(0.18, 0.32)
C	**3**	9.1	4.0 (2.2)	6.8 (2.6)	10.2 (5.5)	(0.20, 0.38)
D	**4**	28.9	20.1 (14.9)	39.2 (25.6)	57.3 (42.4)	(0.21, 0.47)
E	**5**	10.8	7.6 (5.9)	13.0 (8.8)	20.3 (15.8)	(0.20, 0.42)

Efficiency values at 100 cd/m^2 are showed in parentheses. [a)] Maximum brightness. [b)] Maximum EQE. [c)] Maximum power efficiency. [d)] Maximum current efficiency. [e)] 1931 CIE chromaticity calculated from EL spectra at 9 V.

Conclusions

It was shown, that donor substituents have significant influence on photophysical and charge-transporting properties of donor-acceptor-donor type *para*-substituted diphenylsulfone derivatives. The nature of a donor also affects electroluminescent performances of the respective devices containing the newly synthesized diphenylsulfone derivatives as the hosts. The compounds demonstrated relatively high triplet levels (2.99-3.12 eV). Among the synthesized compounds, bis(4-(4-methoxy-9*H*-carbazole-9-yl)phenyl)sulfone demonstrated the best hosting properties, which can

be explained by its relatively high hole mobility (2.8×10^{-4} cm^2/Vs at electric field of $5.6\cdot10^5$ V/cm) and high photoluminescence quantum yield (87%) of its molecular mixture the emitter exhibiting thermally activated delayed fluorescence. Using this host, green thermally activated delayed fluorescence organic light emitting diode was fabricated with brightness of 28.9 thousand cd/m^2 and maximum external quantum efficiency of 20.1%. The device showed power and current efficiencies of 25.6 lm/W and 42.4 cd/A respectively at operating brightness of 100 cd/m^2.

Acknowledgements

DG acknowledges to the ERDF PostDoc project No. 1.1.1.2/VIAA/1/16/177. This work was supported by the project of scientific co-operation program between Latvia, Lithuania and Taiwan "Polymeric Emitters with Controllable Thermally Activated Delayed Fluorescence for Solution-processable OLEDs" (grant No. S-LLT-19-4).

References

[1] Tang CW, Vanslyke SA. Organic electroluminescent diodes. Appl Phys Lett 1987;51:913–5. doi:10.1063/1.98799.

[2] Koden M. OLED display. OLED Displays and Lightning 2017, p. 127–46. doi:10.1002/9781119040477.ch8.

[3] Baldo MA, O'Brien DF, You Y, Shoustikov A, Sibley S, Thompson ME, et al. Highly efficient phosphorescent emission from organic electroluminescent devices. Nature 1998;395:151–4. doi:10.1038/25954.

[4] Endo A, Sato K, Yoshimura K, Kai T, Kawada A, Miyazaki H, et al. Efficient up-conversion of triplet excitons into a singlet state and its application for organic light emitting diodes. Appl Phys Lett 2011;98: 083302. doi:10.1063/1.3558906.

[5] Wong MY, Zysman-Colman E. Purely organic thermally activated delayed fluorescence materials for organic light-emitting diodes, Adv Mater 2017, 29, 1605444. doi.org/10.1002/adma.201605444.

[6] Zhang Q, Li J, Shizu K, Huang S, Hirata S, Miyazaki H, et al. Design of efficient thermally activated delayed fluorescence materials for pure blue organic light emitting diodes. J Am Chem Soc 2012;134:14706–9. doi:10.1021/ja306538w.

[7] Uoyama H, Goushi K, Shizu K, Nomura H, Adachi C. Highly efficient organic light-emitting diodes from delayed fluorescence. Nature 2012;492:234–8. doi:10.1038/nature11687.

[8] Witzel H, Pindur U. Reactions of electron-rich heterocycles with orthocarboxylic acid derivatives. 11. Reactions of carbazole and 4-methoxycarbazole with triethyl orthoformate: Regiospecific functionalization of the carbazole nucleus. J Heterocyclic Chem 1988;25:907–10. doi:10.1002/jhet.5570250339.

[9] Hladka I, Lytvyn R, Volyniuk D, Gudeika D, Grazulevicius JV. W-shaped bipolar derivatives of carbazole and oxadiazole with high triplet energies for electroluminescent devices. Dyes Pigments 2018;149:812–21. doi:10.1016/j.dyepig.2017.11.043.

[10] Miyamoto E, Yamaguchi Y, Yokoyama M. Ionization potential of organic pigment film by atmospheric photoelectron emission analysis. Electrophotography 1989;28:364–70. doi:10.11370/ISJEPJ.28.364.

[11] Amorim CA, Cavallari MR, Santos G, Fonseca FJ, Andrade AM, Mergulhão S. Determination of carrier mobility in MEH-PPV thin-films by stationary and transient current techniques. J Non Cryst Solids 2012;358:484–91. doi:10.1016/j.jnoncrysol.2011.11.001.

[12] Sun C, Ran X, Wang X, Cheng Z, Wu Q, Cai S, et al. Twisted molecular structure on tuning ultralong organic phosphorescence. J Phys Chem Lett 2018;9:335–9. doi:10.1021/acs.jpclett.7b02953.

[13] a) Onsagbr L. Electric moments of molecules in liquids. J Am Chem Soc 1936;58:1486–93. doi:10.1021/ja01299a050; b) Barker JA, Watts RO. Monte carlo studies of the dielectric properties

of water-like models. Mol Phys 1973;26:789–92. doi:10.1080/00268977300102101; c) Watts RO. Monte carlo studies of liquid water. Mol Phys 1974;28:1069–83. doi:10.1080/00268977400102381.

[14] a) Lippert E. Spektroskopische bestimmung des dipolmomentes aromatischer verbindungen im ersten angeregten singulettzustand. Zeitschrift für elektrochemie, Berichte Der Bunsengesellschaft Für Phys Chemie 1957;61:962–75. doi:10.1002/bbpc.19570610819; b) Mataga N, Kaifu Y, Koizumi M. Solvent effects upon fluorescence spectra and the dipolemoments of excited molecules. Bull Chem Soc Jpn 1956;29:465–70. doi:10.1246/bcsj.29.465.

[15] Copp SM, Faris A, Swasey SM, Gwinn EG. Heterogeneous solvatochromism of fluorescent DNA-stabilized silver clusters precludes use of simple Onsager-based stokes shift models. J Phys Chem Lett 2016;7:698–703. doi:10.1021/acs.jpclett.5b02777.

[16] Hong Y, Lam JWY, Tang BZ. Aggregation-induced emission. Chem Soc Rev 2011;40:5361–88. doi:10.1039/c1cs15113d.

[17] Chen Y, Lam JWY, Kwok RTK, Liu B, Tang BZ. Aggregation-induced emission: Fundamental understanding and future developments. Mater Horizons 2019;6:428–33. doi:10.1039/c8mh01331d.

[18] Leung NLC, Xie N, Yuan W, Liu Y, Wu Q, Peng Q, et al. Restriction of intramolecular motions: The general mechanism behind aggregation-induced emission. Chem - Eur J 2014;20:15349–53. doi:10.1002/chem.201403811.

[19] Nakanotani H, Masui K, Nishide J, Shibata T, Adachi C. Promising operational stability of high-efficiency organic light-emitting diodes based on thermally activated delayed fluorescence. Sci Rep 2013;3. doi:10.1038/srep02127.

[20] Lee DR, Kim BS, Lee CW, Im Y, Yook KS, Hwang SH, et al. Above 30% external quantum efficiency in green delayed fluorescent organic light-emitting diodes. ACS Appl Mater Interfaces 2015;7:9625–9. doi:10.1021/acsami.5b01220.

[21] D'Andrade BW, Datta S, Forrest SR, Djurovich P, Polikarpov E, Thompson ME. Relationship between the ionization and oxidation potentials of molecular organic semiconductors. Org Electron Physics, Mater Appl 2005;6:11–20. doi:10.1016/j.orgel.2005.01.002.

[22] Byeon SY, Lee DR, Yook KS, Lee JY. Recent progress of singlet-exciton-harvesting fluorescent organic light-emitting diodes by energy transfer processes. Adv Mater 2019: 1803714. doi:10.1002/adma.201803714.

[23] Bässler H. Charge transport in disordered organic photoconductors. Phys Status Solidi 1993;175:15–56. doi:10.1002/pssb.2221750102.

[24] Chatterjee T, Wong KT. Perspective on host materials for thermally activated delayed fluorescence organic light emitting diodes. Adv Opt Mater 2019;7. doi:10.1002/adom.201800565.

[25] Im Y, Lee JY. Recent progress of green thermally activated delayed fluorescent emitters. J Inf Disp 2017;18:101–17. doi:10.1080/15980316.2017.1333046.

[26] Etherington MK, Gibson J, Higginbotham HF, Penfold TJ, Monkman AP. Revealing the spin-vibronic coupling mechanism of thermally activated delayed fluorescence. Nat Commun 2016;7. doi:10.1038/ncomms13680.

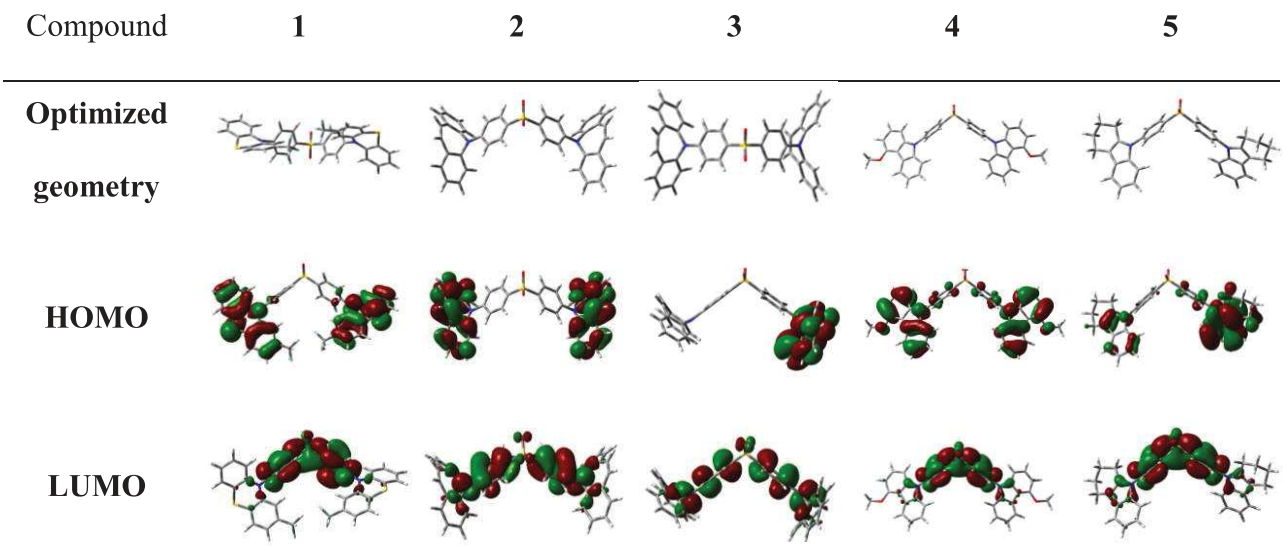

Figure 1. Optimized geometries and HOMO/LUMO of derivatives **1-5** calculated at B3LYP/6-31(d,p) level in vacuum.

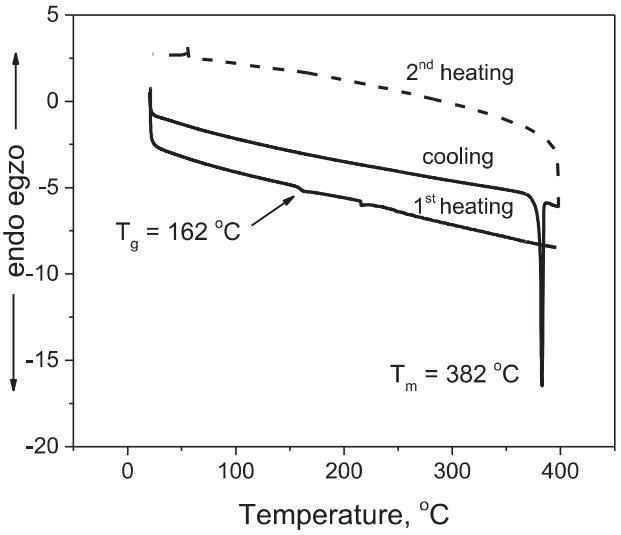

Figure 2. DSC thermograms of compound **3**.

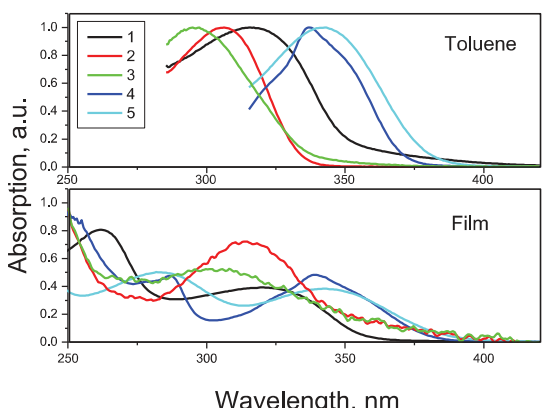

(a)

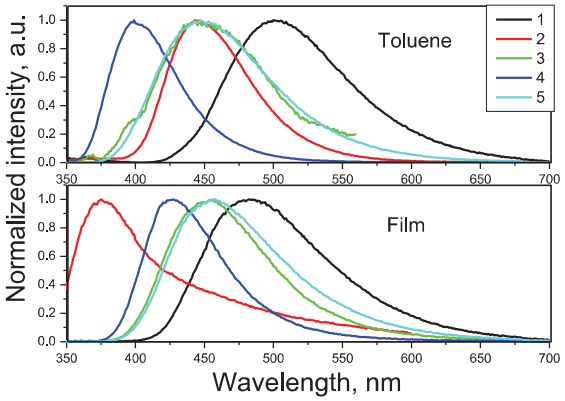

(b)

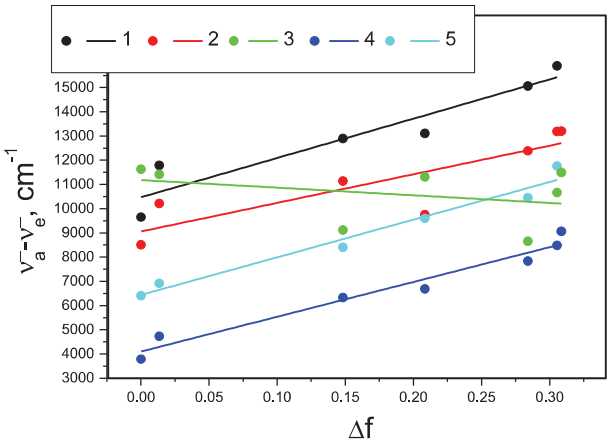

(c)

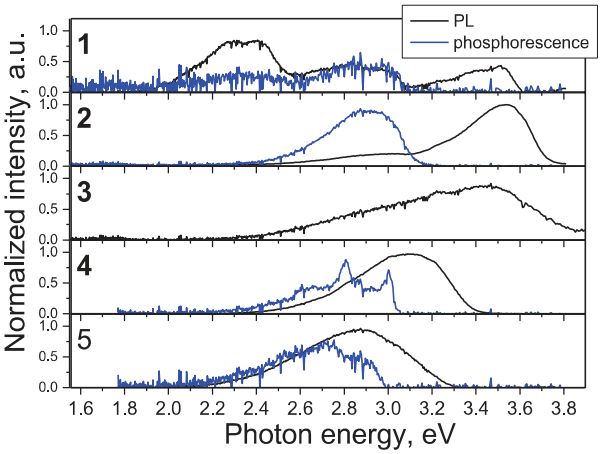

(d)

Figure 3. 1-5: (a) Absorption spectra of neat thin films and dilute toluene solutions. (b) PL spectra of neat thin films and dilute toluene solutions. (c) Lippert-Mataga plot showing the relation bettween Stokes shift and orientation polarisability of the different solvents. (d) PL and phosphorescence spectra of dilute THF solutions recorded at 77 K.

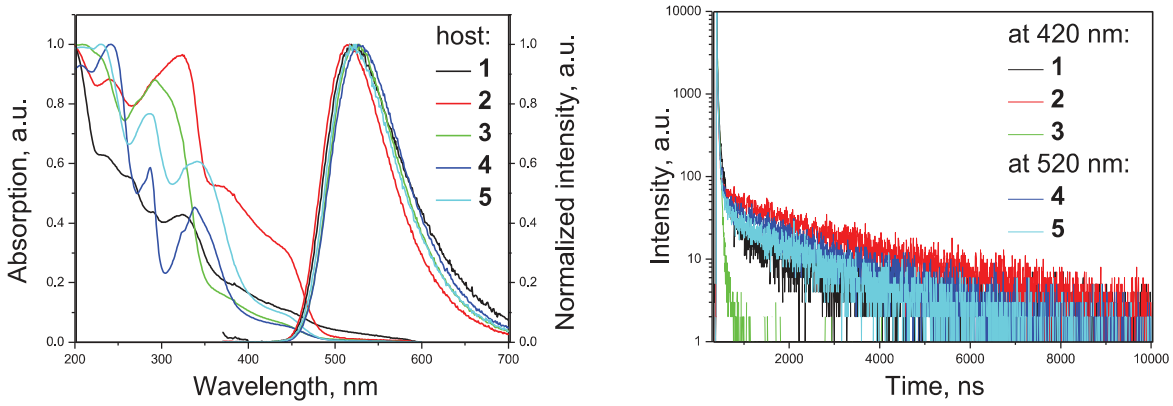

(a) (b)

Figure 4. Absorption and PL spectra (a) and PL decay curves of thin films of 5wt% solid solutions of 4CzIPN in **1-5**.

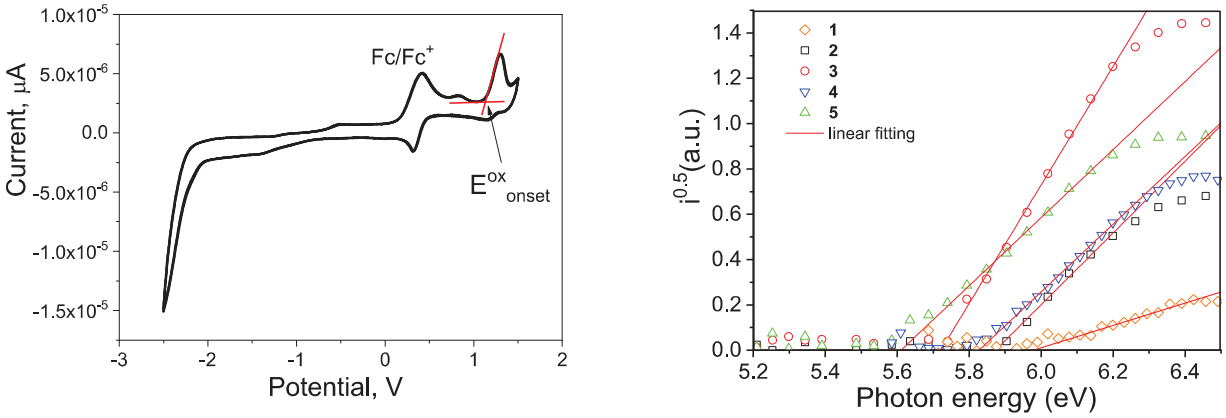

(a) (b)

Figure 5. (a) Cyclic voltammograms of dilute solution of derivative **3** in dry dichloromethane (scan rate 100 mV/s). (b) Electron photoemission spectra of compounds **1-5** recorded in air.

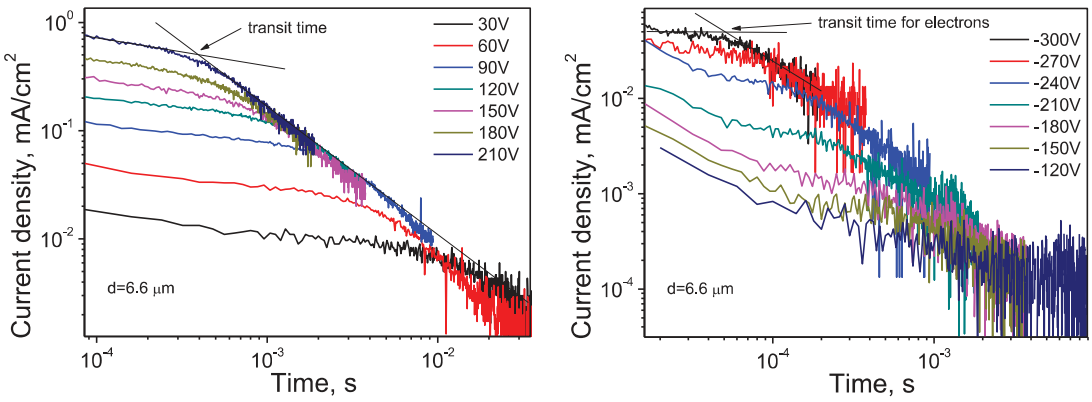

(a) (b)

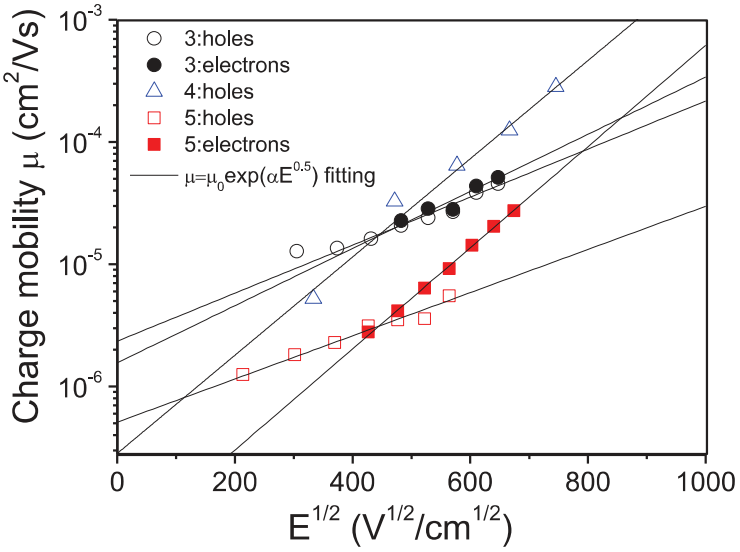

(c)

Figure 6. Photocurrent transients of holes (a) and electrons (b) for vacuum-deposited film of compound **5** and electric field dependences of charge mobilities for the layers of compounds **3-5** (c). Fitting was performed according Poole–Frenkel type mobility ($\mu = \mu_0 e^{\alpha E^{0.5}}$ where μ_0 is zero-field mobility; α is field dependence parameter, and E is electric field [23].

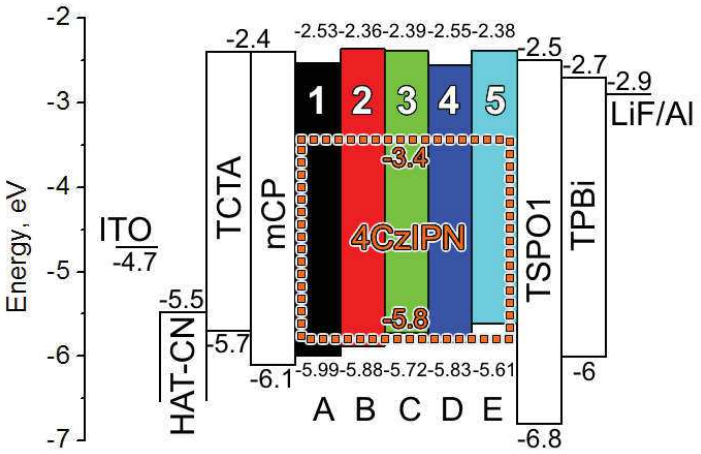
Energy, eV
-2
-3
-4
-5
-6
-7
ITO
-4.7
HAT-CN
-5.5
TCTA
-2.4
-5.7
mCP
-6.1
-2.53-2.36-2.39-2.55-2.38
1
2
3
4
5
-3.4
4CzIPN
-5.8
-5.99-5.88-5.72-5.83-5.61
A B C D E
TSPO1
-2.5
-6.8
TPBi
-2.7
-6
LiF/Al
-2.9

(a)

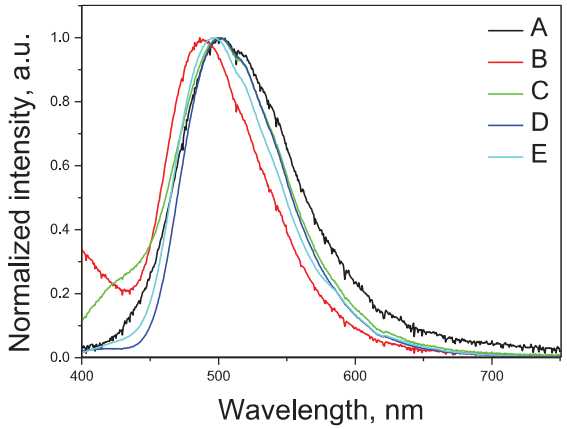
Normalized intensity, a.u.
1.0
0.8
0.6
0.4
0.2
0.0
400
500
600
700
Wavelength, nm
A
B
C
D
E

(b)

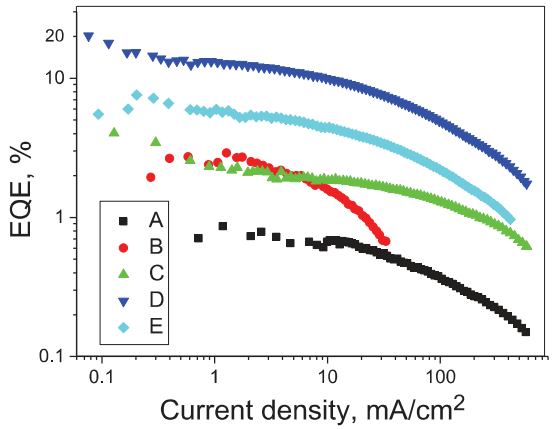
EQE, %
20
10
1
0.1
0.1
1
10
100
Current density, mA/cm2
A
B
C
D
E

(c)

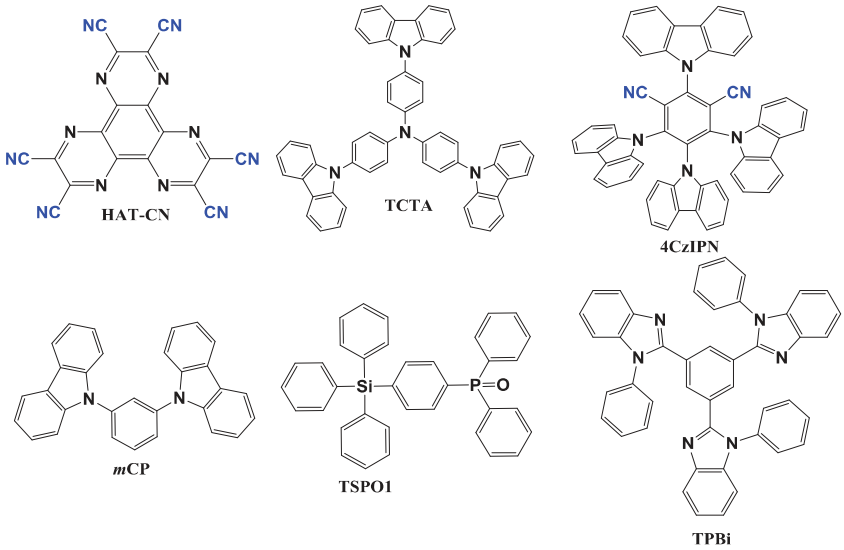
NC
CN
HAT-CN
TCTA
4CzIPN
mCP
Si
P=O
TSPO1
TPBi

(d)

Figure 7. Energy level diagram of the materials of organic layers of OLEDs A-E estimated from the E_g^{opt} and IP values (a), EL spectra recorded at 9 V (b) EQE-current density characteristics (c) and molecular structures of the organic compounds used in the devices (d).

Table 1. Thermal characteristics of derivatives **1-5**.

Derivative	T_m, [°C][a] (scan rate of 10 °C/min)	T_g, [°C][b]	$T_{d\text{-}5\%}$, [°C][c] (scan rate of 20 °C/min)
1	288	103	385
2	199	68	339
3	382	162	433
4	251	141	406
5	224	121	405

[a] T_m - melting temperature (nitrogen atmosphere). [b] T_g - glass-transition temperature, second heating scan. [c] $T_{d\text{-}5\%}$ - 5% weight loss temperature (nitrogen atmosphere).

Table 2. Photophysical data derived from spectral measurements.

Compound	Φ_{THF}[a]	Φ_{tol}[a]	Φ_{film}[b]	Φ_{4CzIPN}[c]	Lifetimes[d], ns	Slopes[e], 10^3 cm^{-1}	E_g^{opt}[f], eV	E_{S1}[g], eV	E_{T1}[g], eV	ΔE_{ST}[g], eV
1	0.02	0.02	0.12	0.22	1.8, 4.2	16.2	2.53	3.60 (2.96)	3.08 (2.85)	0.52 (0.11)
2	0.56	0.33	0.2	0.76	0.5, 6.4	11.8	2.36	3.73 (3.17)	3.12 (2.66)	0.61 (0.51)
3	~0.0001	~0.0001	0.13	0.29	3.5, 13.7, 36.9	-3.2	2.39	3.87 (3.14)	- (2.66)	- (0.48)
4	0.49	0.43	0.49	0.87	4.9, 11.3	14.4	2.55	3.38 (3.31)	3.03 (3.01)	0.35 (0.30)
5	0.22	0.33	0.27	0.28	3.5, 11.5	15.5	2.38	3.29 (3.22)	2.99 (2.95)	0.30 (0.27)

[a] PLQY values of deoxygenated dilute solutions of compounds. [b] PLQY values of neat films of compounds. [c] PLQY values of thin films of 4CzIPN doped in compounds (5wt%). [d] Calculated from PL decay curves of neat films of compounds (Figure S13). [e] Slopes of Lippert-Mataga plots. [f] E_g^{opt} is the onset wavelength of UV absorption spectrum of films. [g] Estimated from onsets of emission spectra of dilute tetrahydrofuran solutions recorded at 77 K. The theoretical values of E_{T1}, ΔE_{ST}, E_{S1} are depicted in parentheses.

Table 3. Oxidation potential, HOMO/LUMO energies, electron affinities, ionization potentials and of derivatives **1-5**.

Derivative	E_{onset}^{ox} vs Fc, [V]	IP_{CV}[a], HOMO[c] [eV]	EA_{CV}[b], LUMO[c] [eV]	E_g^{opt}, [eV][d]	I_p^{PES}, [eV][e]	I_p^{PES}, [eV][f]
1	0.54	5.35/-5.41	1.85/-1.87	3.50	5.99	2.53
2	0.82	5.74/-5.29	2.02/-1.48	3.72	5.88	2.28
3	0.78	5.69/-5.29	2.06/-1.47	3.63	5.72	2.15
4	0.58	5.41/-5.41	2.06/-1.60	3.35	5.83	2.56
5	0.31	5.03/-5.35	1.78/-1.63	3.25	5.61	2.41

[a] $IP_{CV} = |-(1.4\times1e^{-}\times E_{onset}^{ox}$ *vs* Fc/V) − 4.6| eV [21]. [b] $EA_{CV} = -(|IP_{CV}|-E_g^{opt})$ (E_{onset}^{ox}-onset oxidation potential *vs.* the Fc/Fc^{+}. [c] Theoretically estimated HOMO/LUMO levels. [d] $E_g^{opt} = 1240/\lambda_{edge}$, where λ_{edge} is the onset wavelength of UV absorption spectrum of the dilute toluene solution (Table 2). [e] I_p^{PES} is the ionization potential of thin solid layers estimated by photoelectron emission spectrometry. [f] E_A^{PES} is electron affinity for the samples in solid-state.

Table 4. Characteristics of OLEDs.

Device	Host	L_{max}[a], 10^3 cd/m^2	EQE_{max}[b], %	PE_{max}[c], lm/W	CE_{max}[d], cd/A	$CIE_{x,y}$[e]
A	**1**	2.2	0.8 (0.7)	0.9 (0.7)	2.1 (1.7)	(0.23, 0.43)
B	**2**	0.5	2.9 (2.7)	2.9 (2.6)	6.0 (5.7)	(0.18, 0.32)
C	**3**	9.1	4.0 (2.2)	6.8 (2.6)	10.2 (5.5)	(0.20, 0.38)
D	**4**	28.9	20.1 (14.9)	39.2 (25.6)	57.3 (42.4)	(0.21, 0.47)
E	**5**	10.8	7.6 (5.9)	13.0 (8.8)	20.3 (15.8)	(0.20, 0.42)

Efficiency values at 100 cd/m^2 are showed in parentheses. [a)] Maximum brightness. [b)] Maximum EQE. [c)] Maximum power efficiency. [d)] Maximum current efficiency. [e)] 1931 CIE chromaticity calculated from EL spectra at 9 V.

Supporting Information

Diphenylsulfone-based hosts for electroluminescent devices: effect of donor substituents

Oleksandr Bezvikonnyi[a], Dalius Gudeika[a,b], Dmytro Volyniuk[a], Martins Rutkis[b], Juozas V. Grazulevicius[a*]

[a] *Department of Polymer Chemistry and Technology, Kaunas University of Technology, Radvilenu pl. 19, LT-50254, Kaunas, Lithuania*

[b] *Institute of Solid State Physics, University of Latvia, 8 Kengaraga St., Riga LV-1063, Latvia*

** Corresponding author: juozas.grazulevicius@ktu.lt*

Table of contents

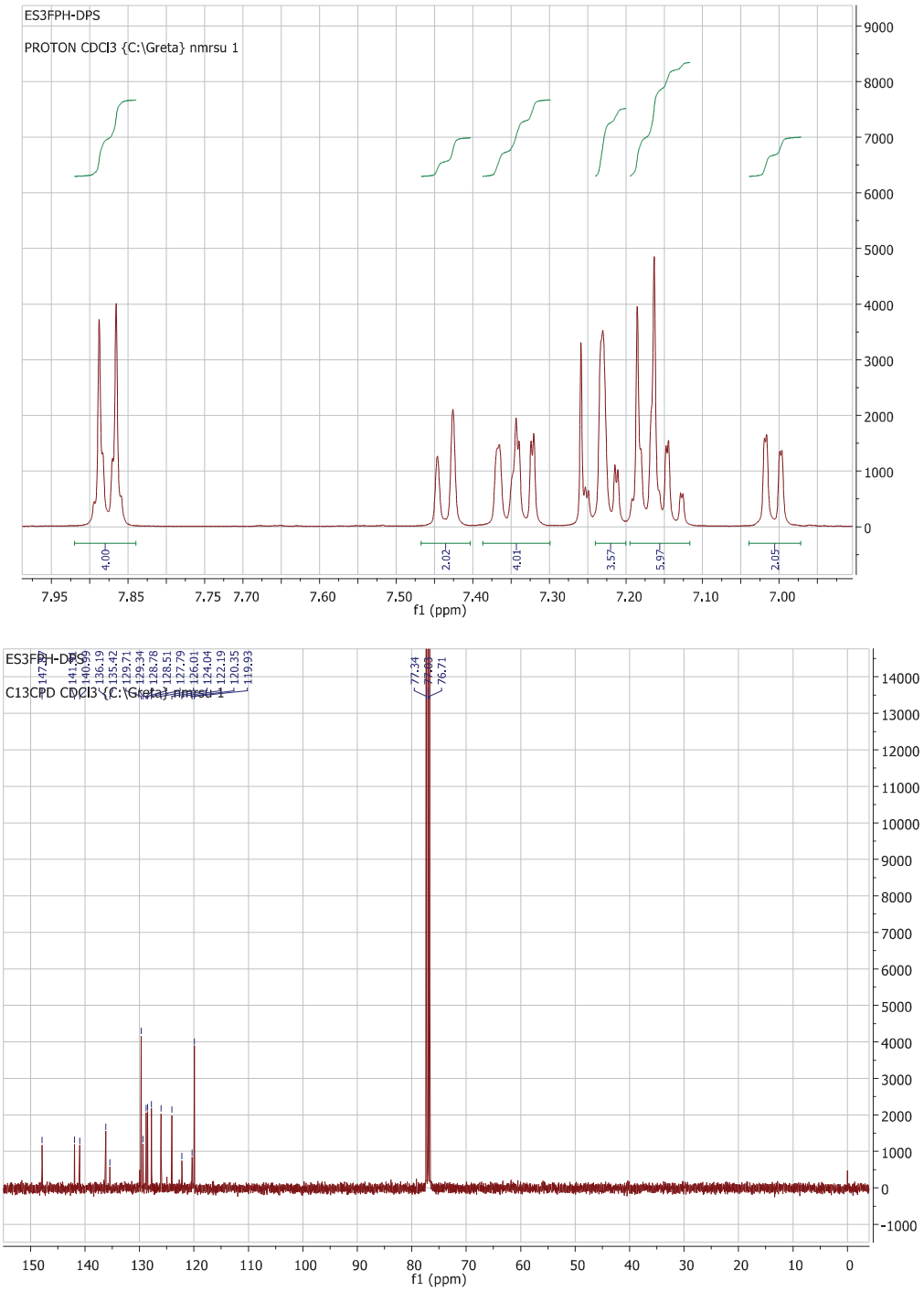

Figure S1. ^{1}H and ^{13}CNMR of **1**.

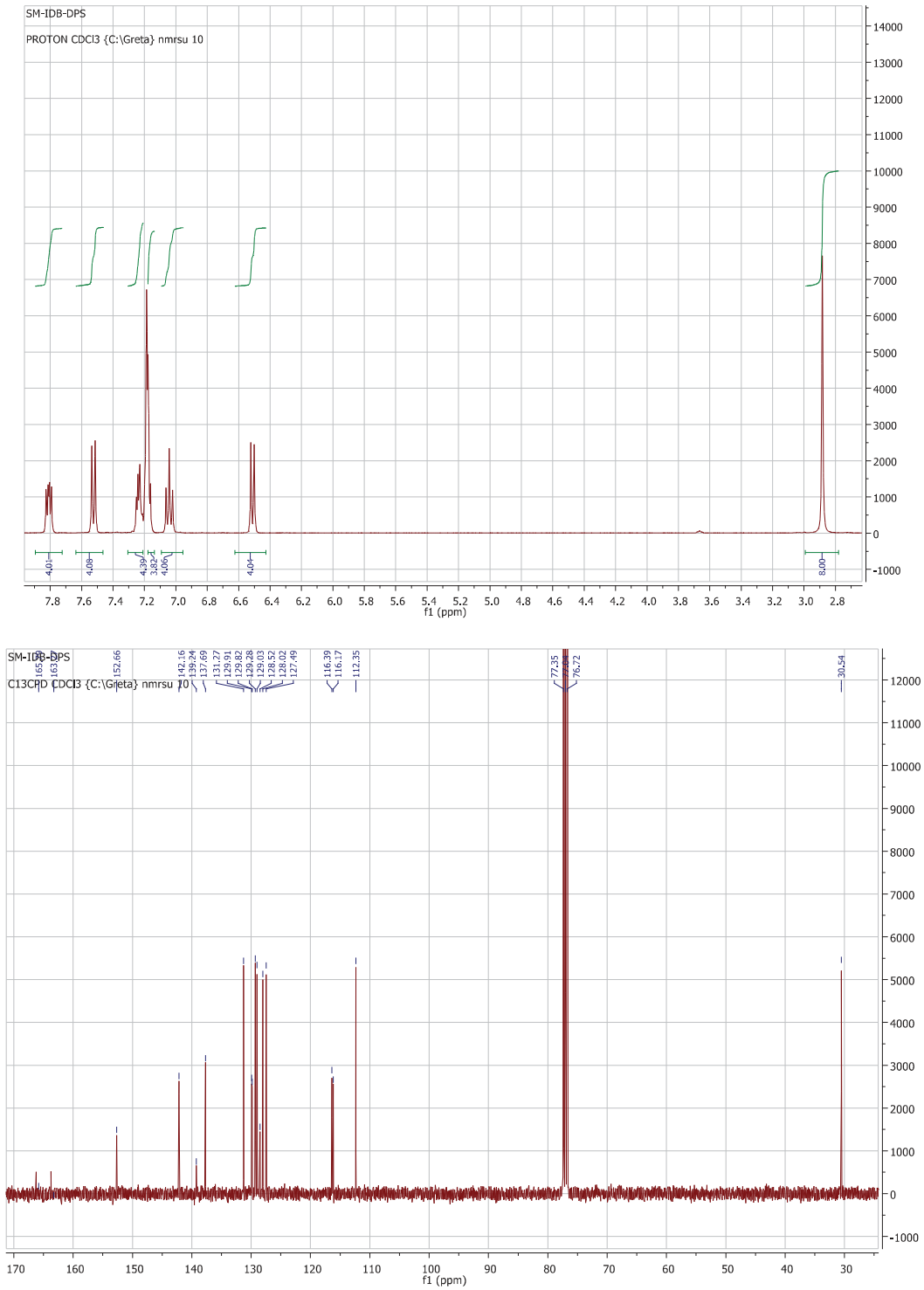

Figure S2. ^{1}H and ^{13}CNMR of **2**.

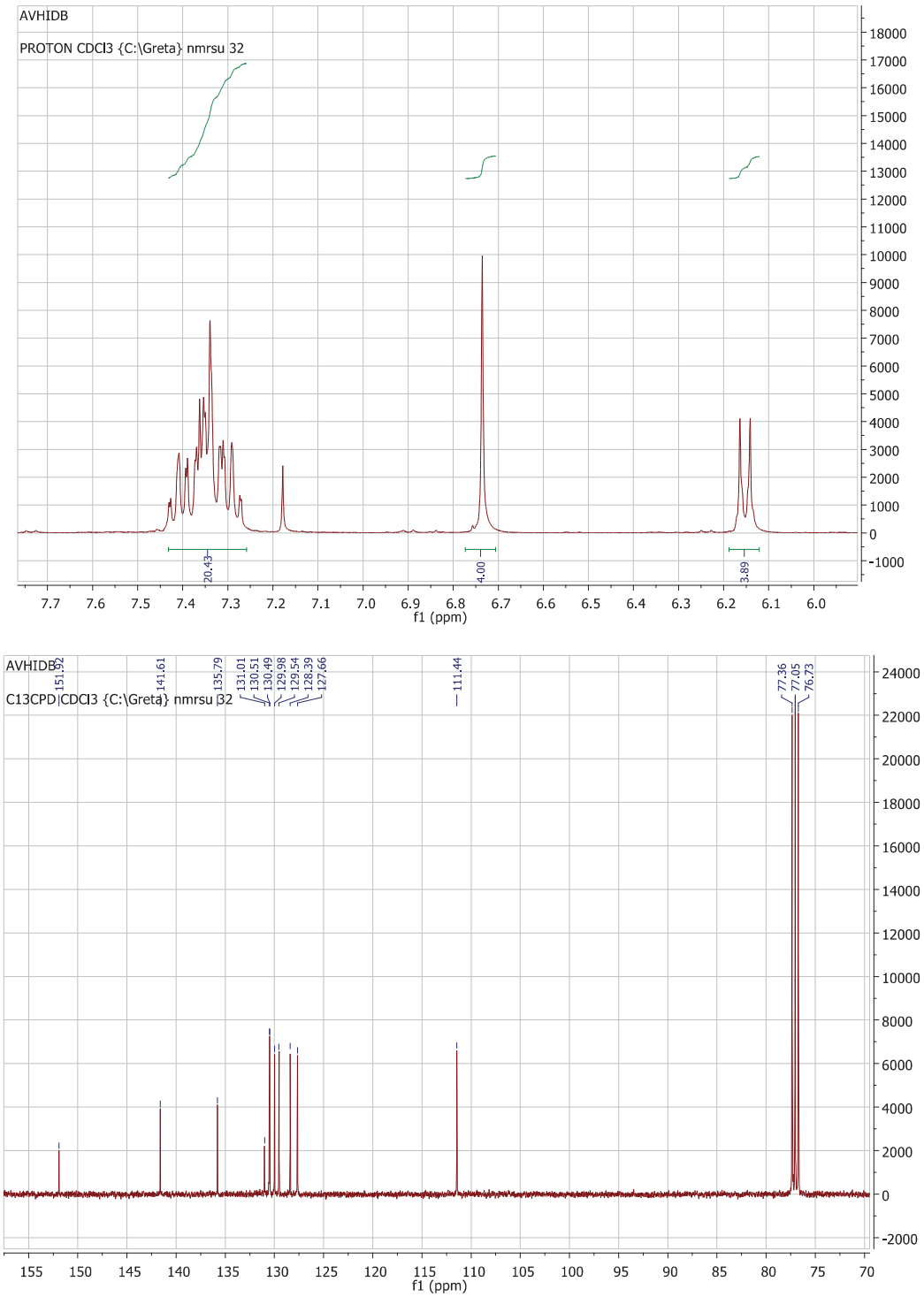

Figure S3. ^{1}H and ^{13}CNMR of **3**.

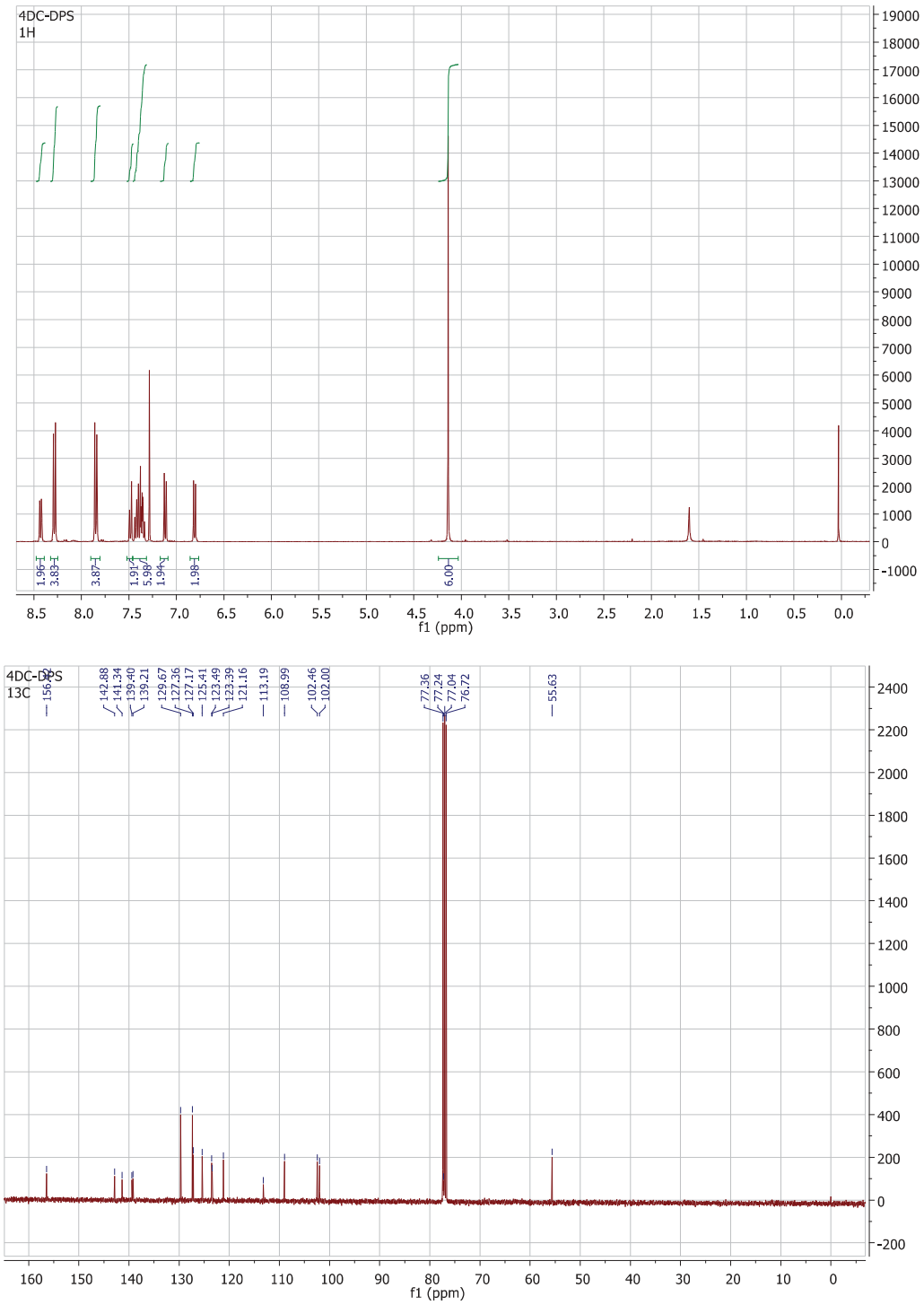

Figure S4. ^{1}H and ^{13}CNMR of **4**.

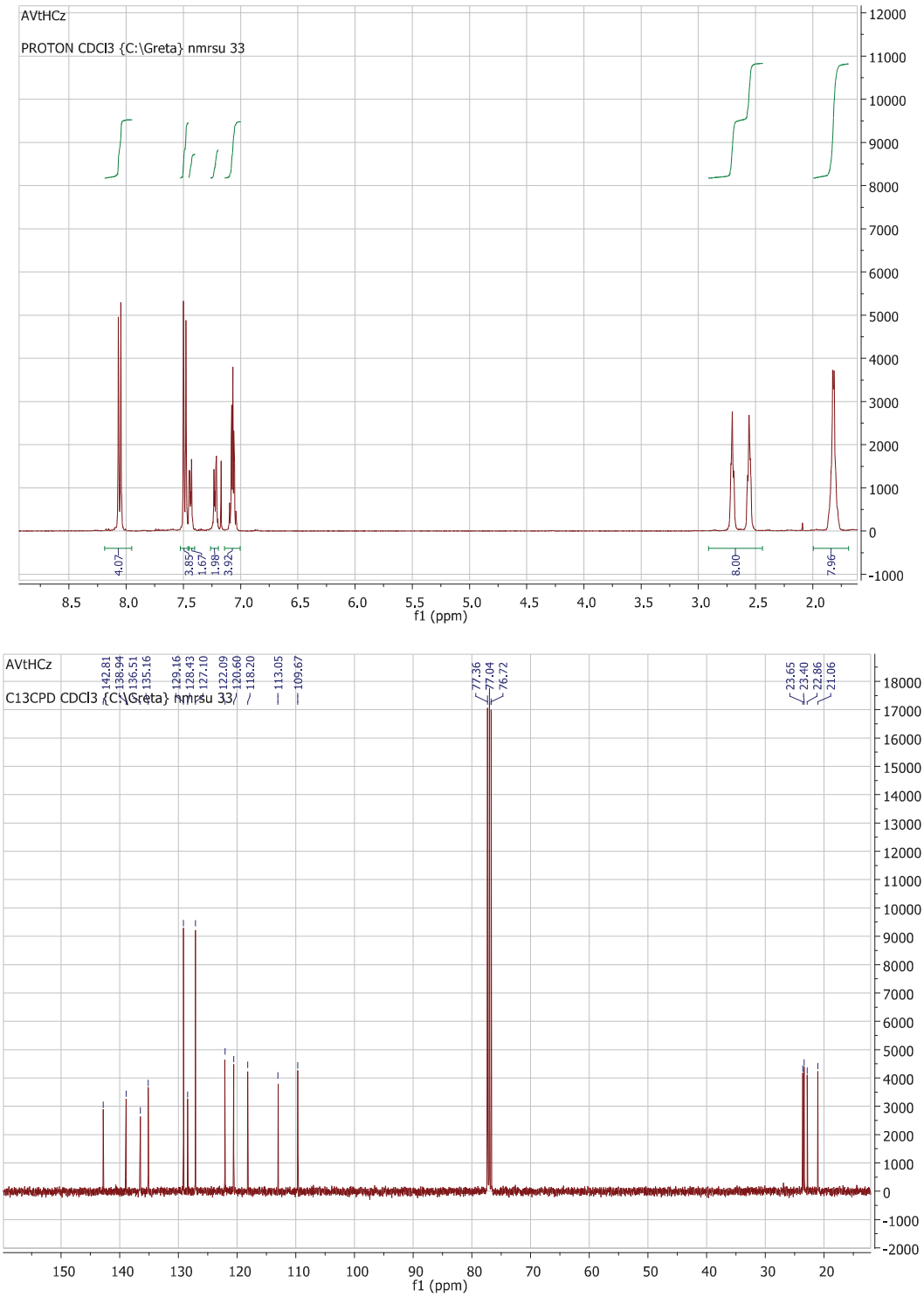

Figure S5. ^{1}H and ^{13}CNMR of **5**.

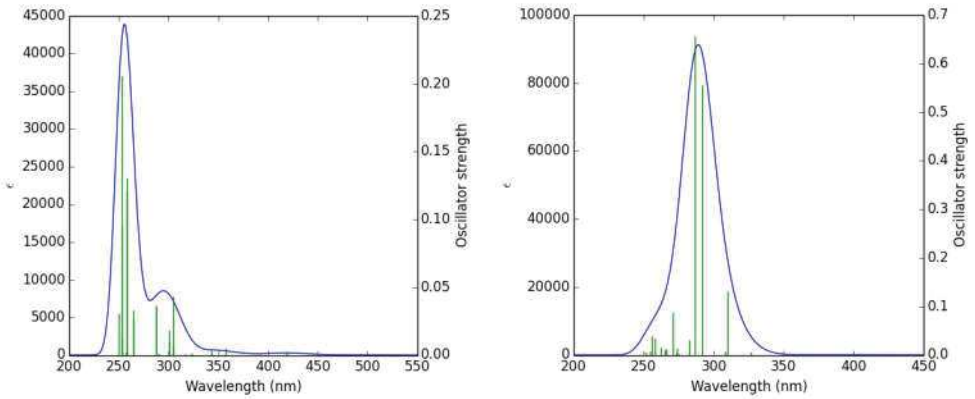

1

2

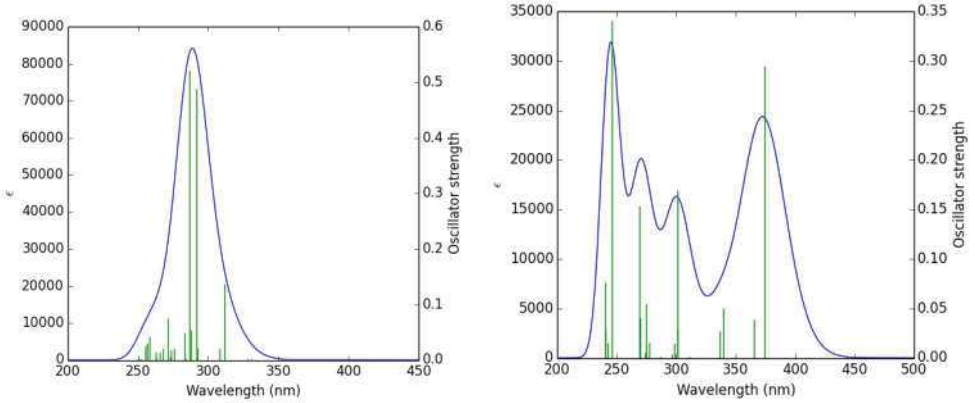

3

4

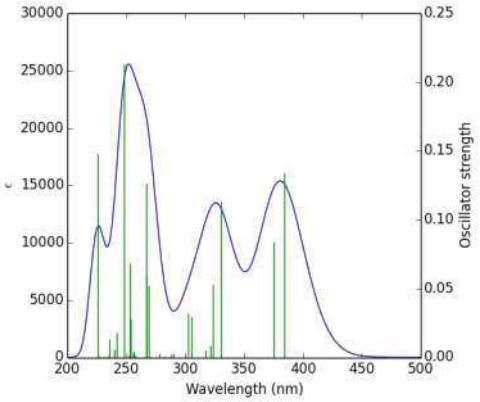

5

Figure S6. The theoretical spectra of **1-5** were obtained by mean of TD-DFT calculations (gas phase). The absorption bands are obtained by considering peak half-widths at half height of 0.3 eV.

Table S1. Theoretical optical characteristics of compounds **1-5**.

Compound	Excitation energy, nm	f[a]	Transition configuration
1	418.83	0.001	H→L (91%)
	357.23	0.0001	H→L+3 (38%) H-1→L+1 (22%) H-1→L+2 (35%)
	305.05	0.0431	H-3→L (14%) H-1→L+6 (35%) H→L+7 (34%) H-1→L+4 (4%) H→L+5 (5%)
2	391.10	0.0011	H-1→L (20%) H→L+1 (79%)
	326.56	0.0054	H-1→L (79%) H→L+1 (21%)
	309.68	0.1307	H-1→L+3 (19%) H→L+2 (78%)
	286.78	0.6568	H→L+4 (87%) H-1→L+7 (3%) H→L+2 (3%) H→L+8 (2%)
3	395.43	0.0006	H-1→L (18%) H→L (81%)
	330.23	0.0026	H-1→L (80%) H→L (19%)
	311.52	0.1367	H→L+2 (79%) H-1→L+2 (8%) H-1→L+3 (9%)
	291.80	0.4887	H-3→L (44%) H-2→L+1 (31%) H-2→L (8%) H→L+5 (4%) H→L+6 (4%)
4	374.59	0.295	H→L (96%) H→L (96%) H→L (96%)

	339.23	0.0509	H-2→L (96%) H-3→L+2 (3%)
	301.45	0.0288	H-1→L+3 (22%) H→L+2 (48%) H→L+4 (18%) H-3→L+6 (3%) H-2→L+7 (3%)
5	384.55	0.1343	H→L (96%)
	330.37	0.1133	H-2→L (96%)
	323.72	0.053	H-3→L (93%) H→L+1 (2%)
	302.28	0.0317	H-1→L+2 (86%) H-1→L+1 (8%)

[a] Oscillator strength.

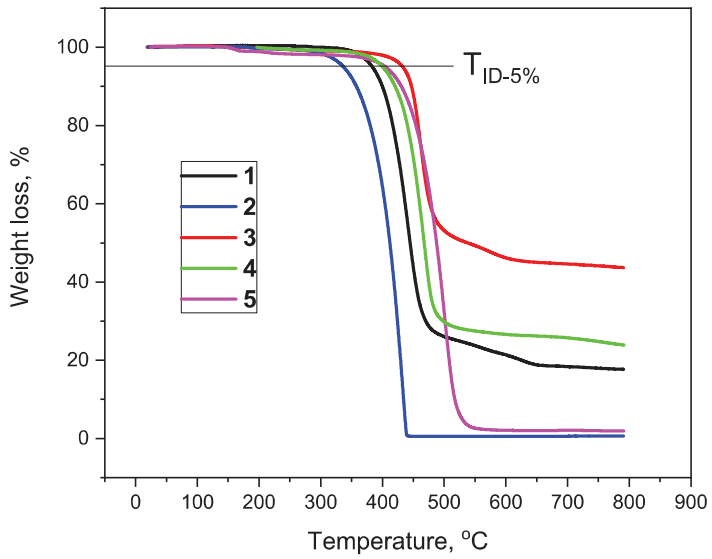

Figure S7. TGA curves of compounds **1-5**.

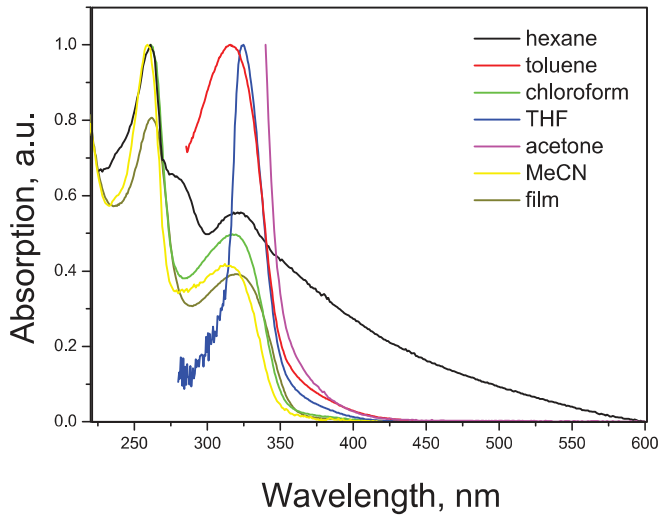

(a)

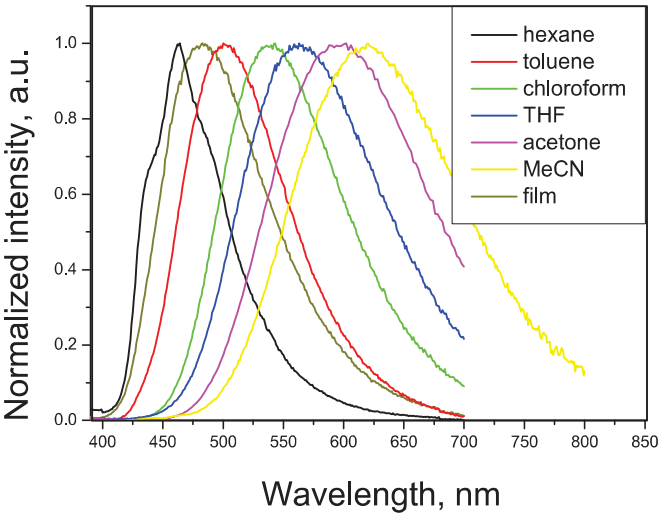

(b)

Figure S8. Dilute solutions and neat film of **1**: (a) Absorption spectra; (b) PL spectra.

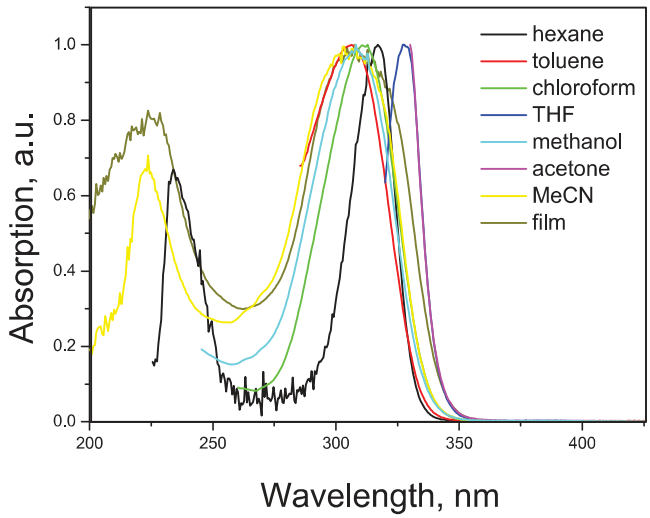

(a)

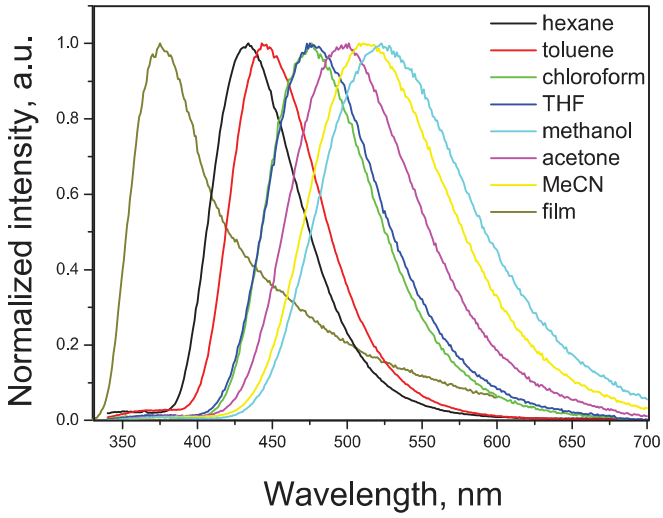

(b)

Figure S9. Dilute solutions and neat film of **2**: (a) Absorption spectra; (b) PL spectra.

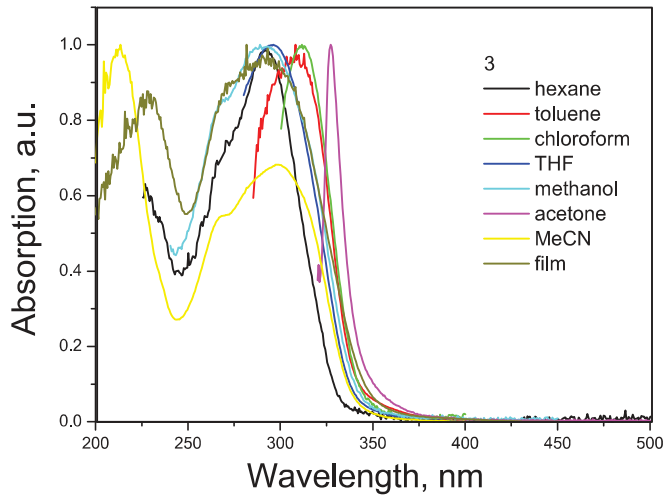

(a)

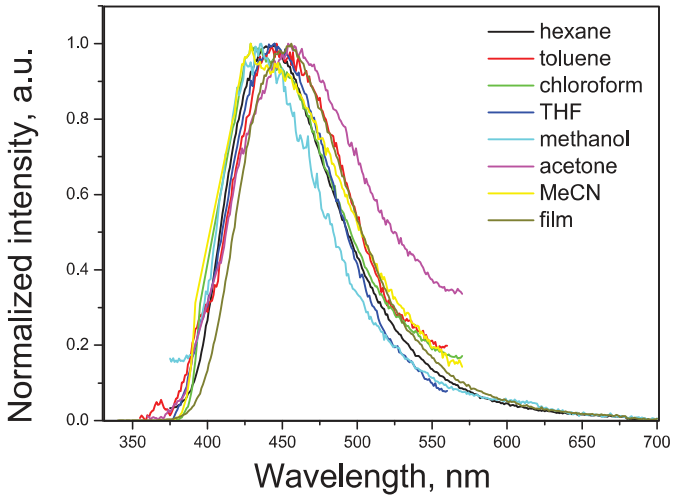

(b)

Figure S10. Dilute solutions and neat film of **3**: (a) Absorption spectra; (b) PL spectra.

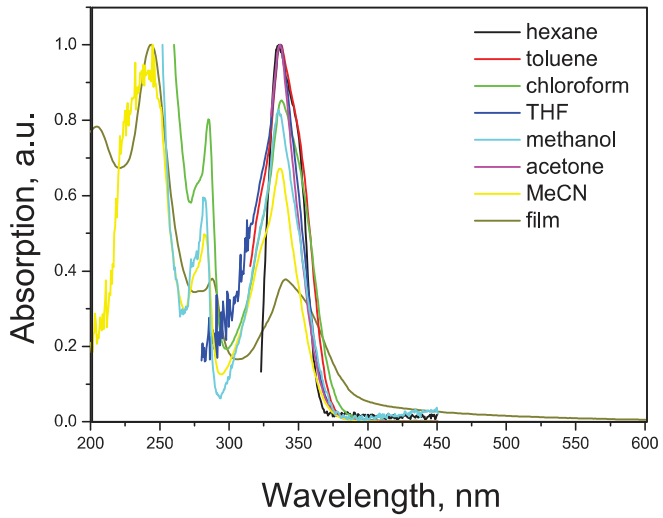

(a)

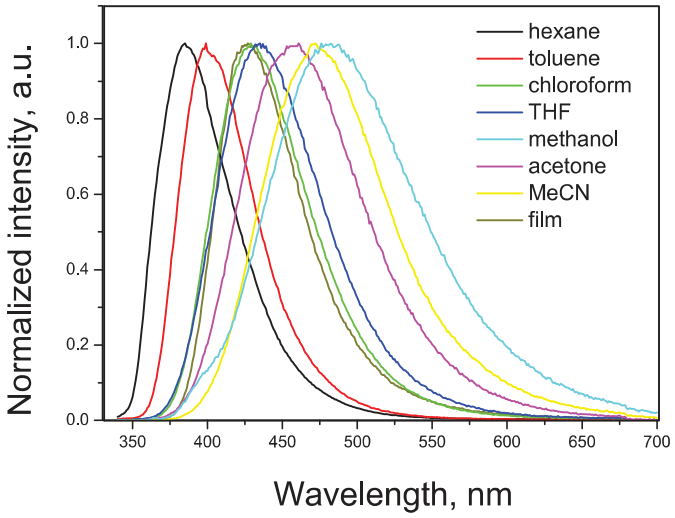

(b)

Figure S11. Dilute solutions and neat film of **4**: (a) Absorption spectra; (b) PL spectra.

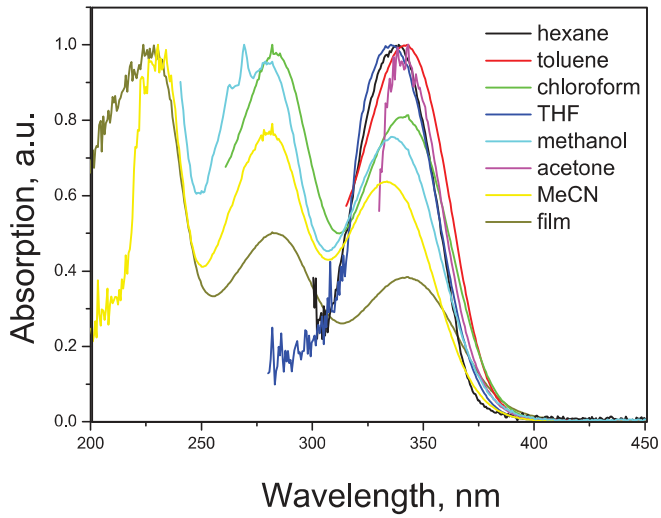

(a)

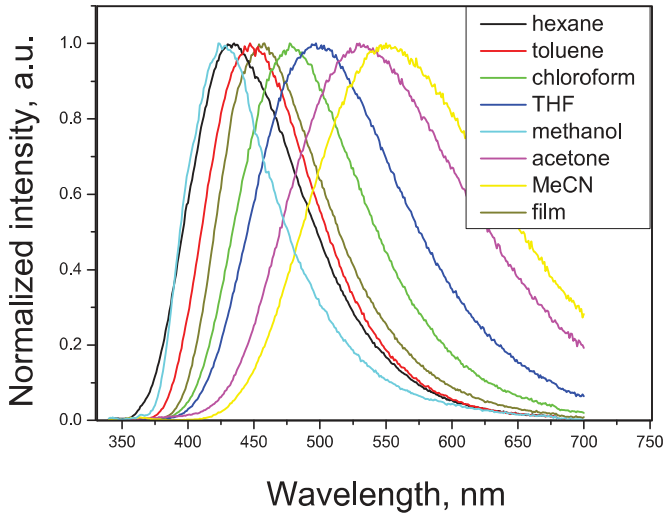

(b)

Figure S12. Dilute solutions and neat film of **5**: (a) Absorption spectra; (b) PL spectra.

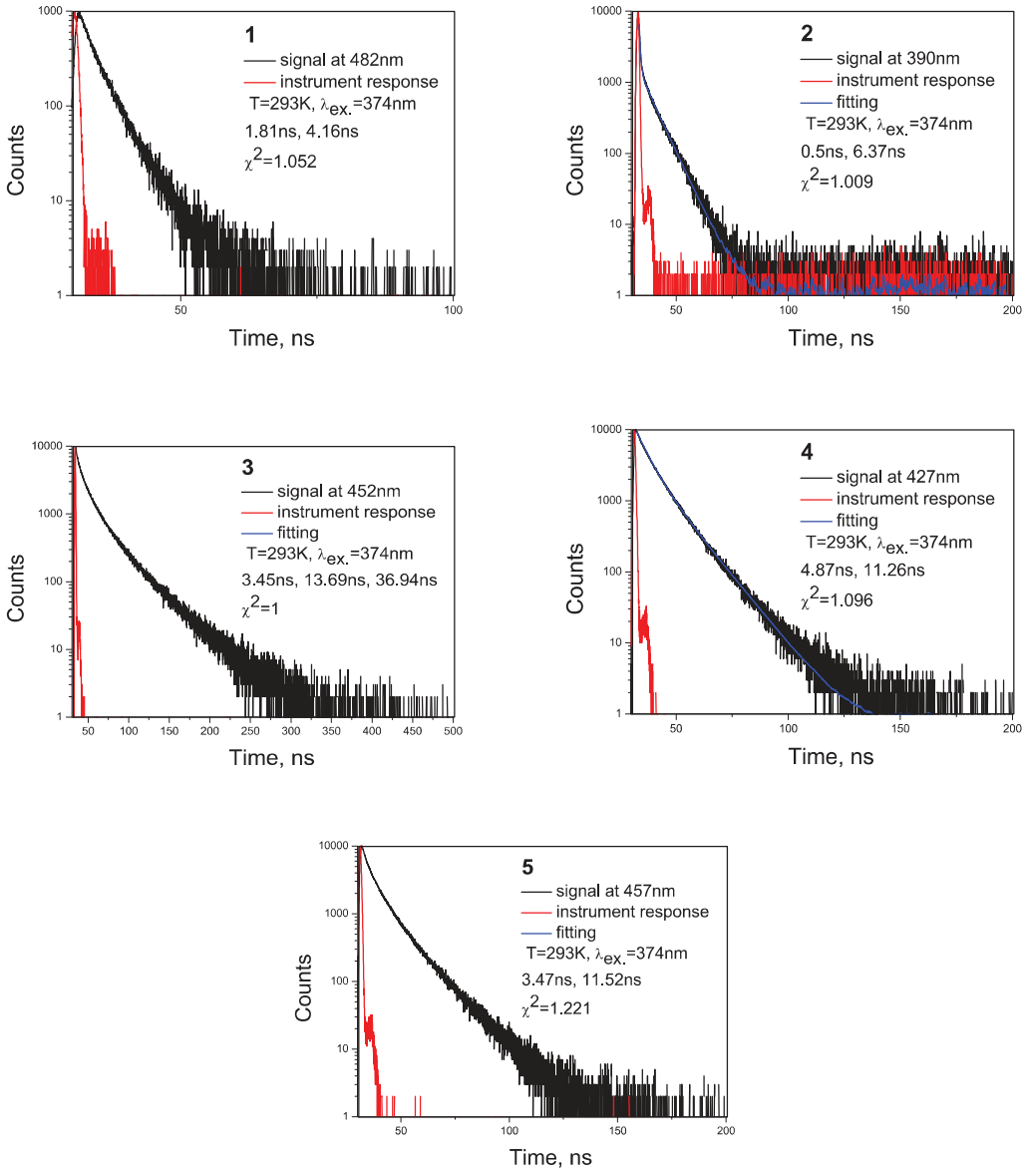

Figure S13. PL decay curves and estimated lifetimes of **1-5** neat films.

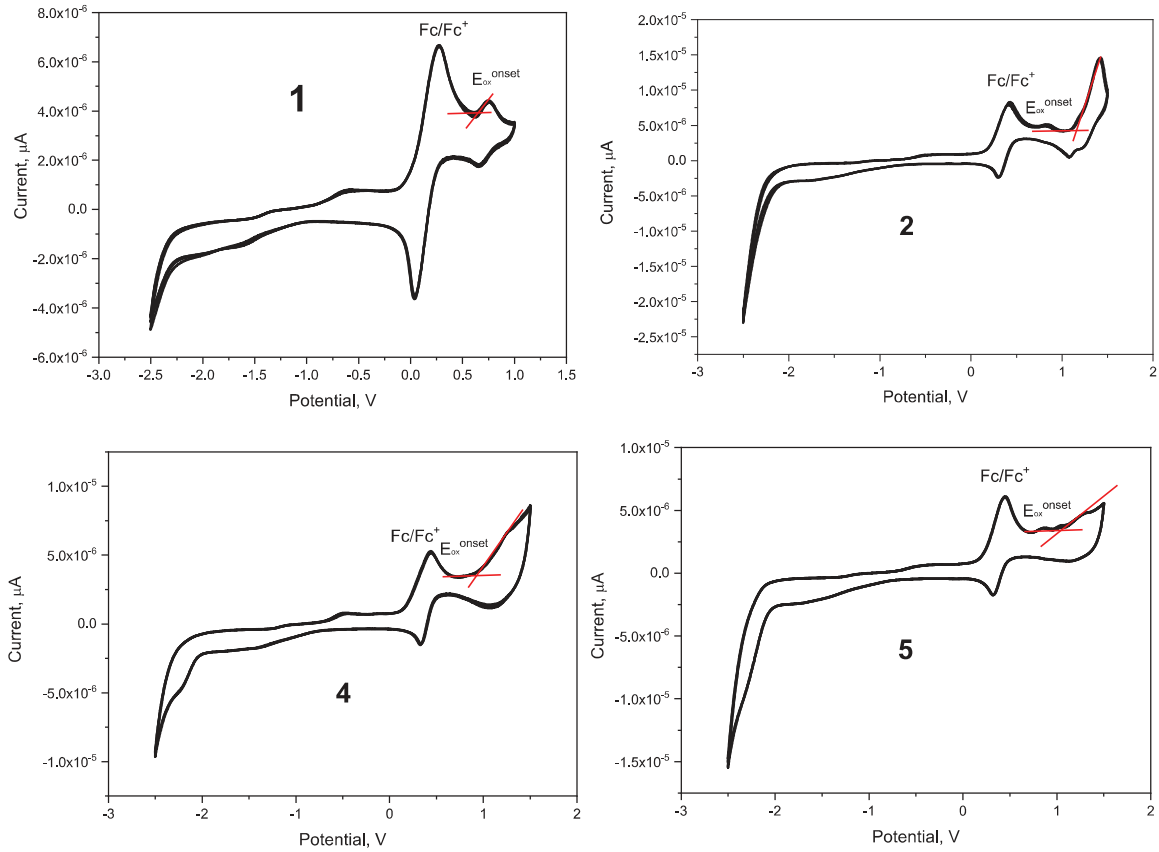

Figure S14. Cyclic voltammograms of dilute solution of compounds **1, 2, 4** and **5** in dichloromethane at sweep rate of 100 mV/s.

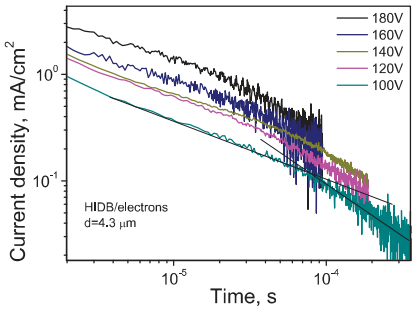
Current density, mA/cm^2
Time, s
HIDB/electrons
d=4.3 μm
180V
160V
140V
120V
100V

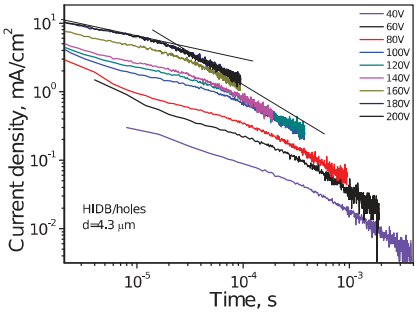
Current density, mA/cm^2
Time, s
HIDB/holes
d=4.3 μm
40V
60V
80V
100V
120V
140V
160V
180V
200V

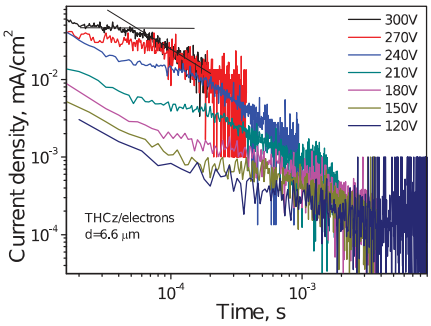
Current density, mA/cm^2
Time, s
THCz/electrons
d=6.6 μm
300V
270V
240V
210V
180V
150V
120V

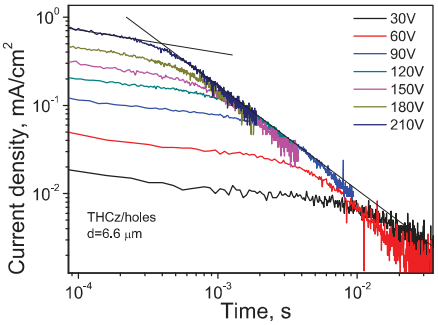
Current density, mA/cm^2
Time, s
THCz/holes
d=6.6 μm
30V
60V
90V
120V
150V
180V
210V

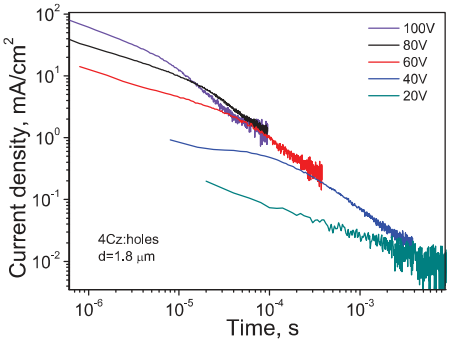
Current density, mA/cm^2
Time, s
4Cz:holes
d=1.8 μm
100V
80V
60V
40V
20V

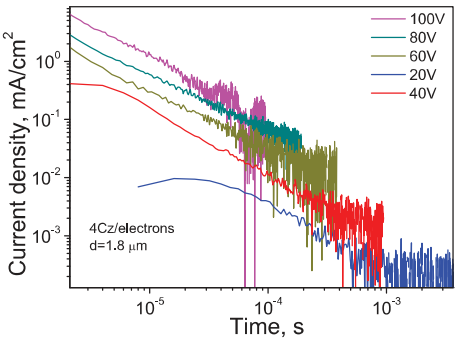
Current density, mA/cm^2
Time, s
4Cz/electrons
d=1.8 μm
100V
80V
60V
20V
40V

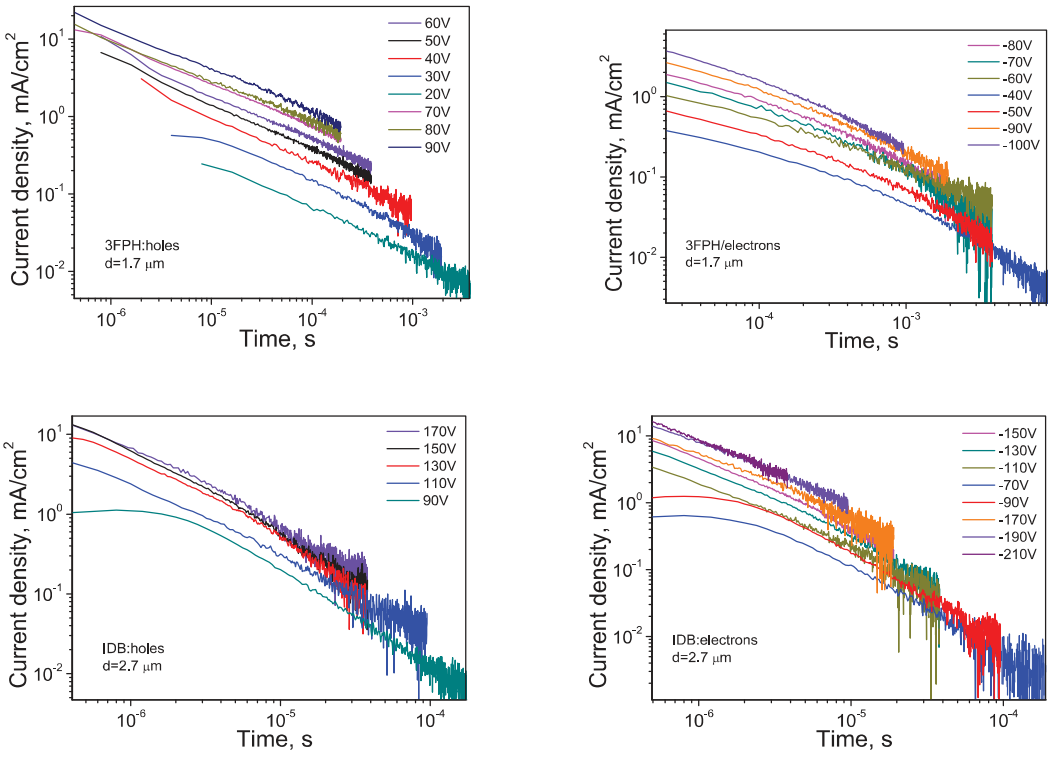

Figure S15. Current transients for the vacuum-deposited films of compounds **1-5**.

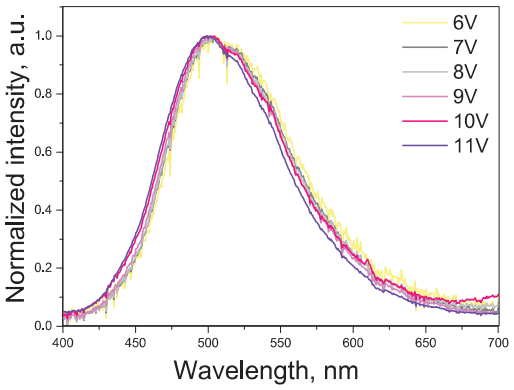

(a)

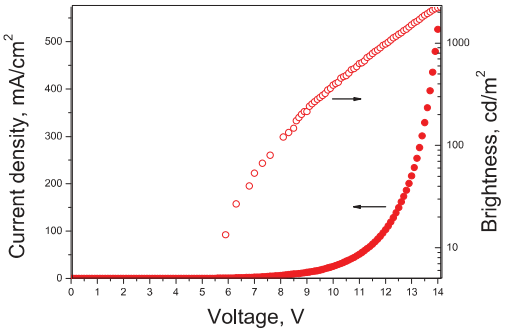

(b)

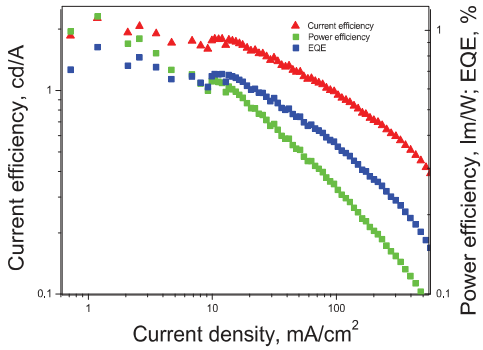

(c)

Figure S16. A OLED: (a) EL spectra recorded at various voltages; (b) Current density and brightness versus voltage correlation; (c) Current, power efficiency and EQE *versus* current density characteristics.

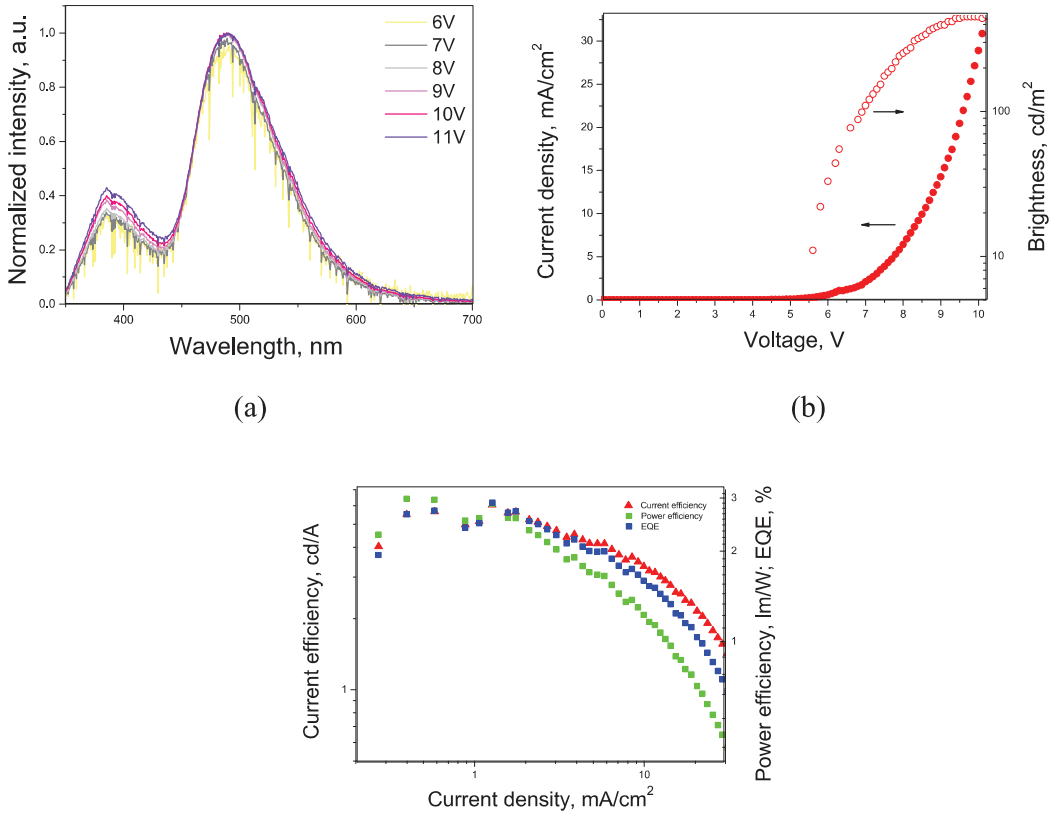

Figure S17. B OLED: (a) EL spectra recorded at various voltages; (b) Current density and brightness versus voltage correlation; (c) Current, power efficiency and EQE *versus* current density characteristics.

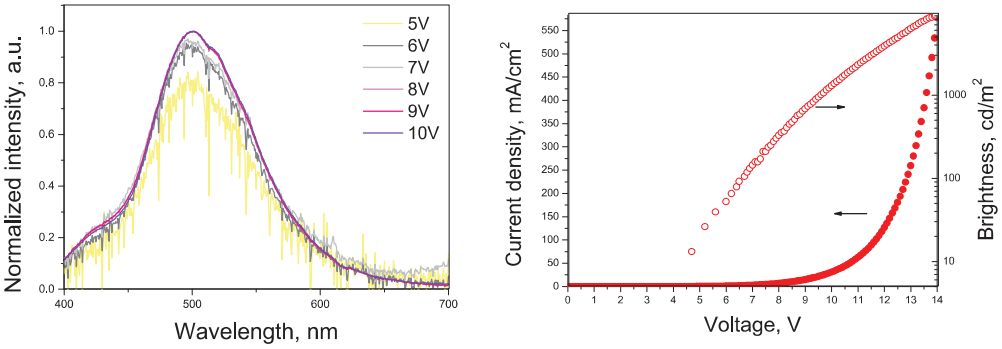

(a) (b)

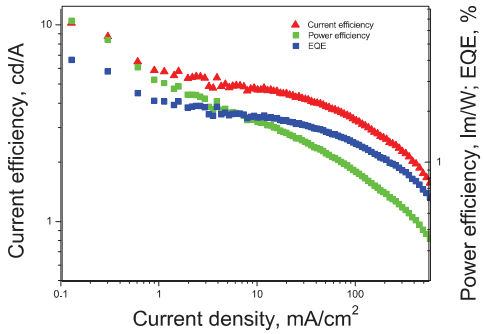

(c)

Figure S18. C OLED: (a) EL spectra recorded at various voltages; (b) Current density and brightness versus voltage correlation; (c) Current, power efficiency and EQE *versus* current density characteristics.

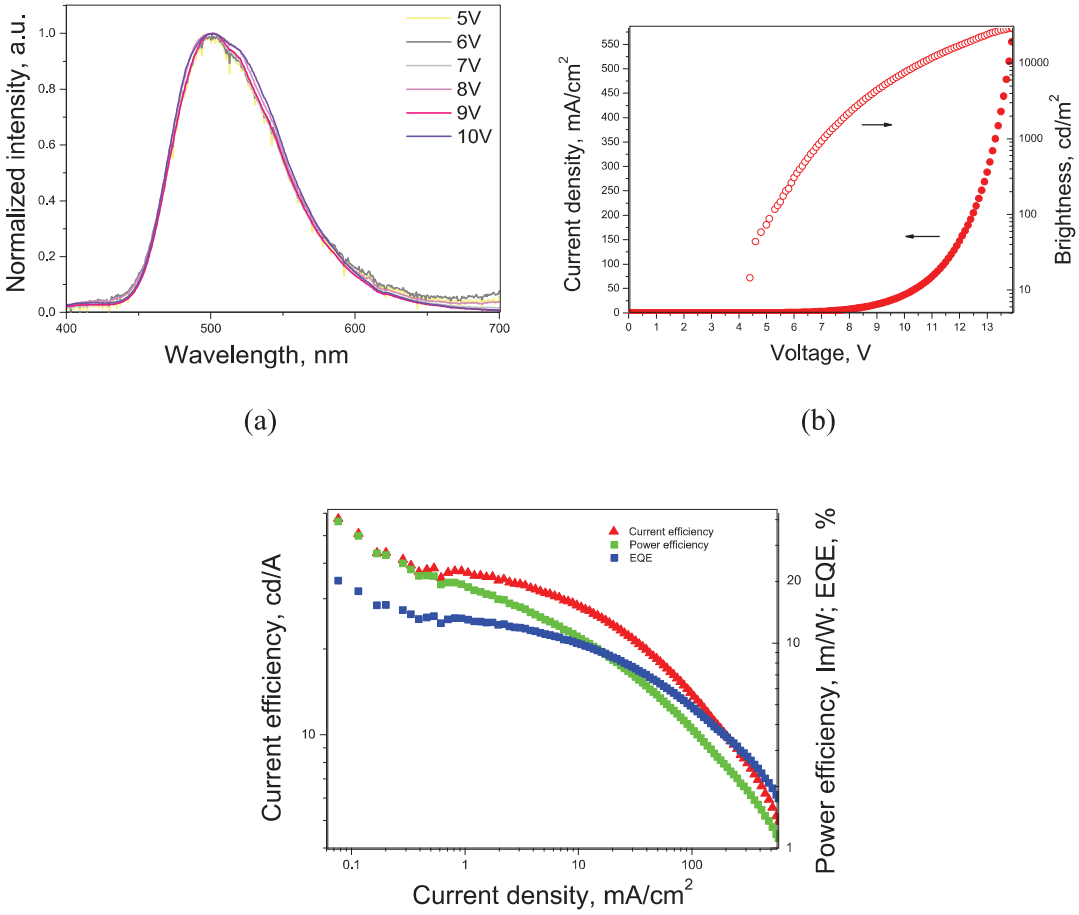

Figure S19. D OLED: (a) EL spectra recorded at various voltages; (b) Current density and brightness versus voltage correlation; (c) Current, power efficiency and EQE *versus* current density characteristics.

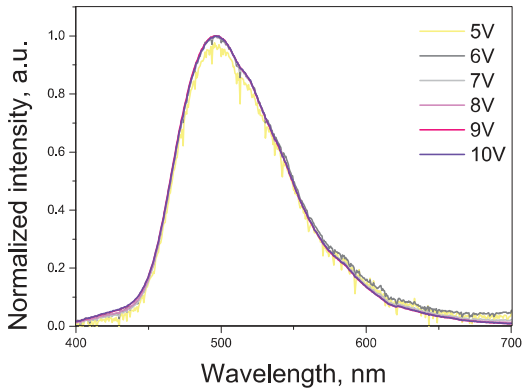

(a)

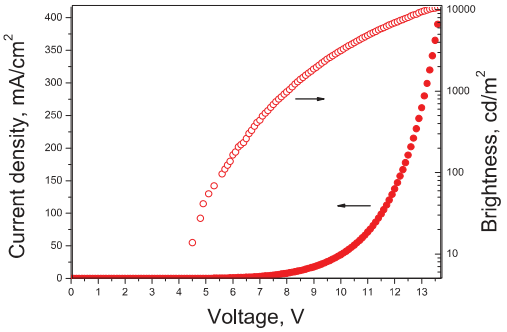

(b)

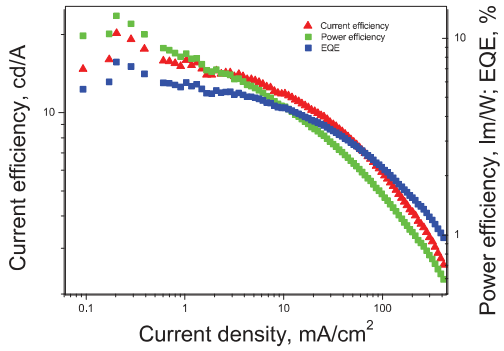

(c)

Figure S20. E OLED: (a) EL spectra recorded at various voltages; (b) Current density and brightness versus voltage correlation; (c) Current, power efficiency and EQE *versus* current density characteristics.

This paper is elaborated at the Centre of Excellence in Advanced Material Research and Technology Transfer of the Institute of Solid State Physics, University of Latvia executing project CAMART² that has received funding from the Horizon 2020 Framework Programme H2020-WIDESPREAD-01-2016-2017-TeamingPhase2 under grant agreement No. 739508